Title	Dynamic Nuclear Polarization at High Temperature for Polarized Proton Target(Dissertation_全文)
Author(s)	Iinuma, Masataka
Citation	Kyoto University (京都大学)
Issue Date	1997-07-23
URL	http://dx.doi.org/10.11501/3128513
Right	
Type	Thesis or Dissertation
Textversion	author

Dynamic Nuclear Polarization at High Temperature for Polarized Proton Target

Masataka Iinuma

A dissertation submitted in partial fulfillment of
the requirements for the degree of

Doctor of Science

Department of Physics
Kyoto University

Abstract

We have carried out the experiment of proton polarization in single crystals of naphthalene and p-terphenyl doped with pentacene using a dye-laser. The experiment has been made in the magnetic field of 3kGauss at room temperature and liquid nitrogen temperature.

The pentacene molecules were excited to the lowest triplet state through singlet excited states with the laser, then the microwave was irradiated during the lifetime of the triplet state and simultaneously the external field was swept for transferring the population difference of electrons between two Zeeman sublevels to the proton polarization by means of the integrated solid effect. It has been confirmed that the 'electron polarization' defined for the two Zeeman sublevels $|0>$ and $|-1>$ on the triplet state is about 70% and that integrated solid effect has worked efficiently.

It has been found that the relaxation rate of protons in the naphthalene crystal increases with laser power significantly at room temperature, whereas it is low but increases slightly with laser power even in liquid nitrogen. The laser power dependence of the relaxation rate during the irradiation of the N_2-laser($\lambda = 337$nm) is larger than that with the dye-laser($\lambda = 595$nm). From these results, we have concluded that it is preferable to irradiate the pulsed dye-laser on the crystal immersed in liquid nitrogen for our purpose.

We obtained the proton polarization of 30% in naphthalene doped with pentacene(0.001mol%) using the pulsed dye-laser with the wavelength of 600nm, the average power of 350mW and the repetition rate of 50Hz at liquid nitrogen temperature. The maximum polarization obtained at room temperature was 0.12%. We obtained the proton polarization of 1.3% and 19% in the single crystal of p-terphenyl doped with 0.1mol% pentacene at room temperature and at liquid nitrogen temperature respectively. The polarization of protons was confirmed by the neutron transmission method. The results were consistent with that measured by means of the NMR method.

We have concluded that the proton polarization by the integrated solid effect on the photoexcited triplet state at high temperature is applicable to the polarized target and the spin filter, since such a target is strong for heating and radiation damage and can be used for very low energy particles as well.

Contents

Chapter 1

Introduction

1.1 Polarized proton targets for particle and nuclear physics

The polarized proton target is useful for particle and nuclear physics. For studying the spin structure of nucleon and fundamental symmetries, measurements of spin correlation parameters in nucleon-nucleon, meson-nucleon and lepton-nucleon scatterings have been made using polarized proton targets. The polarized targets have also been used as slow-neutron polarizers in which the spin directions of the transmitted neutrons have been selected.

The proton polarization according to the Boltzmann distribution in thermal equilibrium is 0.5% in the magnetic field of 25kGauss at the temperature of 0.5K. In order to obtain higher polarization, the method of dynamic nuclear polarization(DNP), using the "solid effect"[1, 2, 3, 4], has been applied, in which the high polarization of the electron in paramagnetic impurities has been transferred to the proton spin by means of microwave irradiation. Since the magnetic moment of the electron is 658 times as large as that of the proton, the thermal polarization of the free electron is 99.8% in 25kGauss at 0.5K.

As target materials, ethylene glycol[5, 6, 7], butanol[8, 9, 10], propanediol[11], and

NH_3[12, 13, 14] have been usually used, since the protons in these materials can be polarized more than 90% in 25kGauss at 0.5K. These materials have an advantage over other materials because of the high density of proton. In addition, they are relatively strong for radiation damage.

In order to polarize protons in these target materials by DNP, the magnetic field higher than 25kGauss with the field homogeneity of 10^{-4} and the temperature below 1K are needed. These conditions give rise to the following problems in scattering experiments.

- The magnetic field of 25kGauss is too high for low momentum particles.
- In order to realize the field homogeneity of 10^{-4} over the target size, a large magnet is necessary. The angular acceptance of such a magnet for incident and scattered particles are limited seriously.
- Complicated cryogenic systems are required to keep the temperature lower than 1K.
- High beam intensity gives the depolarization of protons. The depolarization is caused by heating and radiation damage due to the beam particles.

Since the relaxation time of the proton spin in organic material is quite long at the temperature lower than 0.1K, the proton polarization can be kept for long time in rather low magnetic field without microwave irradiation after the protons are polarized dynamically in higher field. Such a polarized target, called the spin frozen target, is used for many experiments in several institutions in Japan[15, 16, 17, 18], Europe[19, 20, 21] and recently in USA[17, 18, 22].

The spin frozen target allows us to reduce the strength of the magnetic field during the scattering experiment. Furthermore, the field homogeneity of 10^{-4} is not

required for holding the proton polarization. Therefore, large angular acceptance can be provided for incident and scattered particles. However, the spin frozen target needs a dilution refrigerator with high cooling power to keep the temperature of the target below 0.1K. In addition, the temperature increase due to the beam irradiation is serious, since the relaxation time of protons is quite sensitive to the temperature. The radiation damage due to the beam irradiation also leads to the depolarization, since free electrons produced by ionization remain in the crystal for long time without recombination and give rise to the short relaxation time.

Another application of the polarized proton target to particle and nuclear physics is to use as the polarized proton filter with which the slow neutron beam can be polarized, because the proton-neutron scattering cross section has a strong spin dependence below 10MeV. It was shown at Dubna and KEK that the polarized proton target is useful as the neutron polarizer in the epithermal energy region[23, 24]. In the early 1980's, the polarized proton filter was built using ethylene glycol and was installed in an epithermal neutron beam line in KEK[24, 25]. The neutron in the energy region of 1eV has been polarized up to 72% with the proton filter in 25kGauss at 0.5K. A polarized proton filter using ammonia has been constructed in Los Alamos lately. The neutron polarization of about 70% was obtained with the filter in 50kGauss at 1K[26, 27]. In experiments using such polarized filters, the experimental conditions are limited because of the cryogenic system and the high field magnet.

A new method to polarize protons in a low magnetic field without the cryogenic technique has been desired for long time in order to solve above problems.

1.2 Dynamic nuclear polarization on the photoexcited triplet state of aromatic molecules

Triplet states of aromatic molecules excited with light have been investigated for long time[28]. One of the remarkable features of the photoexcited triplet state is the fact that there are population differences among the three Zeeman sublevels of the triplet states[29]. It is caused by the selection rule of the transition from the singlet excited state to the triplet state. Such population differences are almost independent of the strength of the external magnetic field and the temperature.

In 1982, the first experiment of transferring the population differences on the photoexcited triplet states to the proton spin was reported by Kesteren et al.[30]. A single crystal of fluorene doped with phenanthrene was used as a sample for polarizing protons in 3kGauss at 1.2K. The proton polarization was about 3%, which corresponds to the enhancement of 90 compared to the Boltzmann equilibrium polarization. In this case, the proton polarization was obtained by the solid effect, which is not efficient in such a low magnetic field. Lately, in 1985, it was also reported by Kesteren et al. that the polarization of about 42% was obtained in the same kind of crystal in 27kGauss at 1.4K[31]. It was shown that the solid effect is effective also on photoexcited triplet states in a high magnetic field.

A new method for polarization transfer called "Integrated Solid Effect"(ISE) which is effective in low magnetic field, was proposed by Henstra et al. in 1988[32]. In the integrated solid effect the magnetic field is swept during microwave irradiation. In 1990, the first experiment of polarizing proton in a low magnetic field(3kGauss) at room temperature was carried out by means of this method[33]. A single crystal of naphthalene doped with pentacene was used as a sample for polarizing protons. The integrated solid effect was applied to the photoexcited triplet state of pentacene

molecule. The achieved proton polarization of 0.5% corresponds to the enhancement of 5500 compared to the Boltzmann equilibrium polarization. Although this enhancement is surprisingly high in such a low magnetic field and at high temperature, it is still too small for applying to the polarized proton target.

1.3 Dynamic nuclear polarization in low magnetic field at high temperature

In this dissertation we describe our recent experimental results on polarizing protons by means of the dynamic polarization on the photoexcited triplet state in the magnetic field below 10kGauss at the temperature higher than 77K and the possibility of its application to the polarized proton target. The goal of the experiment is the achievement of the high polarization of proton available for scattering experiments without cryogenic technique. Two kinds of aromatic single crystals, naphthalene doped with pentacene and p-terphenyl doped with pentacene are used, since pentacene is easily doped in single crystals of naphthalene and of p-terphenyl. Electrons in a pentacene molecule are diamagnetic in the ground state. They are excited to a higher singlet state with a laser beam. And then the spin-orbit interaction causes the transition from singlet excited states to the intermediate triplet state, where the integrated solid effect is applied for polarizing protons.

A series of experiments have been performed in 3kGauss at room temperature and at liquid nitrogen temperature. In particular, the polarization of 30% in naphthalene has been obtained in 3kGauss at liquid nitrogen temperature. The proton polarization was measured not only by the NMR method but also by the neutron transmission.

It has been found that these materials are applicable to the polarized target and to the polarized proton filter of the slow neutron beam. These targets are expected

to be strong against beam heating and radiation damage due to high beam intensity.

In Chapter 2, an overview of the dynamic polarization of protons is introduced. The principle of DNP with the pentacene molecule is also presented. Then, the experimental procedure and apparatus are described in Chapter 3. In Chapter 4, the experimental results and discussion are presented. The possibility of the application to polarized targets is discussed in Chapter 5. We give the conclusion in Chapter 6.

Chapter 2

Dynamic Polarization of Protons

2.1 Dynamic nuclear polarization by solid effect

The interaction between the spin and magnetic field is known as the Zeeman interaction. In the case of nuclei, which have the magnetic moment of $\boldsymbol{\mu} = \gamma\hbar\boldsymbol{I}$, in the external field $\boldsymbol{H}_0$ along the z-axis, the Zeeman Hamiltonian $\mathcal{H}$ is expressed as

$$\mathcal{H} = -\boldsymbol{\mu}\cdot\boldsymbol{H}_0 = -\gamma\hbar\hat{I}_z H_0, \tag{2.1}$$

where γ is the gyromagnetic ratio, and I_z is the z-component of the nuclear spin. Since protons have the spin of 1/2, there are two Zeeman levels, $m = +1/2$ and $m = -1/2$ as shown in Figure 2.1. We define the polarization as

$$P = \frac{N_+ - N_-}{N_+ + N_-}, \tag{2.2}$$

where N_+ and N_- correspond to the populations on the energy levels of m=+1/2 and m=−1/2 respectively.

In the case of the ensemble of protons in thermal equilibrium, the populations on the both levels obey the Boltzmann distribution. They are expressed as

$$N_+ = \alpha \exp(+\frac{\gamma\hbar H_0}{2kT}),$$

$$N_- = \alpha \exp(-\frac{\gamma\hbar H_0}{2kT}).$$

Here, T is the temperature, and k is the Boltzmann constant, and α is a constant. The degree of the polarization in thermal equilibrium can be expressed as

$$P = \tanh(\frac{\gamma\hbar H_0}{2kT}). \tag{2.3}$$

Since $\gamma/2\pi = 4.2$MHz/kGauss for the proton, the proton polarization P_p is given as

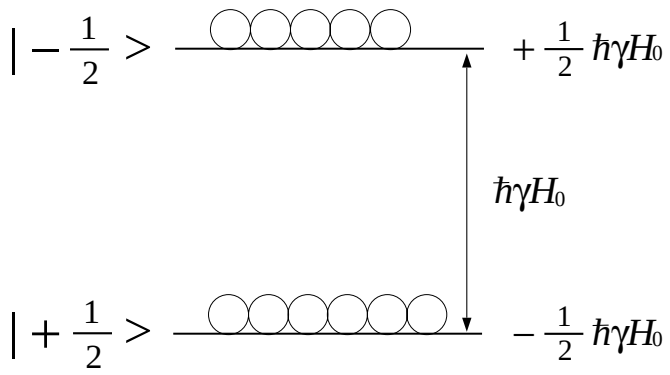

Figure 2.1: Zeeman levels of the free proton in the magnetic field of H_0 along the z-axis

$$P_p = \tanh(1.008\times10^{-4}\frac{H_0}{T})\approx10^{-4}\frac{H_0}{T}, \tag{2.4}$$

where H_0 and T are given in kGauss and K respectively. Here, $10^{-4}H_0/T \ll 1$ is assumed.

In the magnetic field of 25kGauss at the temperature of 0.5K, the polarization is about 0.5%. For obtaining 10% polarization, 100kGauss and 0.1K are required. In the case of electron, $\gamma/2\pi = 2.8\times10^3$MHz/kGauss is given. The electron polarization P_e can be expressed as

$$P_e = \tanh(0.067\frac{H_0}{T}). \tag{2.5}$$

The polarization of electrons is 93% in 25kGauss at 1K in thermal equilibrium.

In the ordinary dynamic nuclear polarization, protons are polarized by transferring the electron polarization to protons. The polarization transfer is performed by irradiation of microwaves. It is caused by the dipole-dipole interaction between a proton and an electron. It is called the "solid effect", of which mechanism is understood as follows.

The spin Hamiltonian of a pair of a proton and an electron is given as

$$\mathcal{H}_0 = \mathcal{H}_S + \mathcal{H}_I + \mathcal{H}_{SI}, \tag{2.6}$$

where $\mathcal{H}_S$ and $\mathcal{H}_I$ are Zeeman terms which express the interaction of the magnetic field $\boldsymbol{H}_0$ with the electron and proton spins respectively. $\mathcal{H}_{SI}$ represents the spin-spin interaction of the electron and proton. This interaction is treated as a perturbation of $\mathcal{H}_S + \mathcal{H}_I$. Since it is the interaction between magnetic moments of the electron and proton, $\mathcal{H}_{SI}$ is given by the dipole-dipole formula

$$\mathcal{H}_{SI} = \gamma_S \gamma_I \hbar^2 \left(\frac{\boldsymbol{S} \cdot \boldsymbol{I}}{r^3} - \frac{3\,(\boldsymbol{S} \cdot \boldsymbol{r})\,(\boldsymbol{I} \cdot \boldsymbol{r})}{r^5} \right). \tag{2.7}$$

Here, γ_S is the gyromagnetic ratio of electron, $\boldsymbol{S}$ is the spin of electron. γ_I is the gyromagnetic ratio of proton, $\boldsymbol{I}$ is the spin of proton. $\boldsymbol{r}$ represents the relative position vector between an electron and a proton, and is expressed by the spherical coordinates, r, θ, φ. According to the perturbation theory of first order, four perturbed states made by the dipole-dipole interaction are shown in Figure 2.2. Here, $|m_S, m_I\rangle$ is the notation showing the z-components of electron spin m_S and proton spin m_I. ω_S and ω_I are the Larmor frequencies of electron and proton respectively. We define q as $-3/4 \cdot \gamma_S \gamma_I \hbar / r^3 \cdot 1/\omega_I \sin\theta \cos\theta e^{-i\varphi}$, q^* as the complex conjugate of q. Since $\omega_S \gg \omega_I$ is fulfilled, the terms including $1/\omega_S$ can be neglected. The transitions of $|+1/2, -1/2\rangle \leftrightarrow |-1/2, -1/2\rangle$ and $|+1/2, +1/2\rangle \leftrightarrow |-1/2, +1/2\rangle$ are allowed, whereas the transitions of $|+1/2, -1/2\rangle \leftrightarrow |-1/2, +1/2\rangle$ and $|+1/2, +1/2\rangle \leftrightarrow$

$|-1/2,-1/2\rangle$ are forbidden without the dipole-dipole interaction. However, the forbidden transitions are allowed slightly, since the dipole-dipole interaction account for a small transition probability between the different spin states. The ratio between

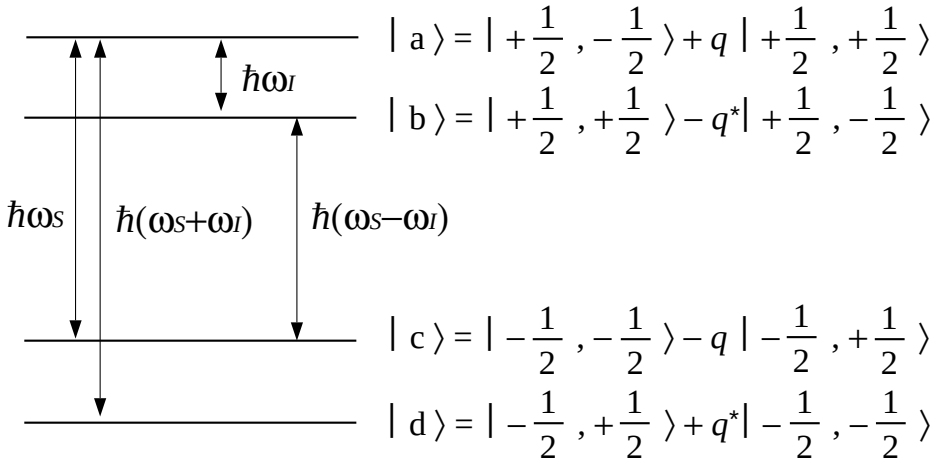

Figure 2.2: Zeeman levels of an electron - proton pair including the hyperfine interaction

the allowed transition W_a and the forbidden transition W_f is

$$\frac{W_f}{W_a} = 4\,|q|^2 = \frac{9}{4}\frac{{\gamma_S}^2{\gamma_I}^2\hbar^2}{r^6}\frac{1}{{\omega_I}^2}\sin^2\theta\cos^2\theta \tag{2.8}$$

We consider an ensemble of electron spins coupled with proton spins and assume that the electrons are polarized according to the Boltzmann distribution. The transition by irradiation of microwaves whose frequencies are $\omega_S+\omega_I$ makes the population of $|a>$ to be equal to $|d>$(See Figure 2.2). Since the spin-lattice relaxation time of the electron spin T_{1e} is much shorter than the relaxation time of proton spin T_{1p}, the transition from $|a>$ to $|c>$ occurs spontaneously within T_{1p}. Then the transition between $|a>$ and $|d>$ continues by microwave irradiation. As the result, the population on $|c>$ becomes much larger than that on $|d>$. Irradiation of microwaves whose frequencies are $\omega = \omega_S - \omega_I$ gives the transition between $|b>$ and $|c>$. In

this case, protons are polarized to the opposite direction to the proton polarization obtained by irradiation of microwaves with $\omega = \omega_S + \omega_I$.

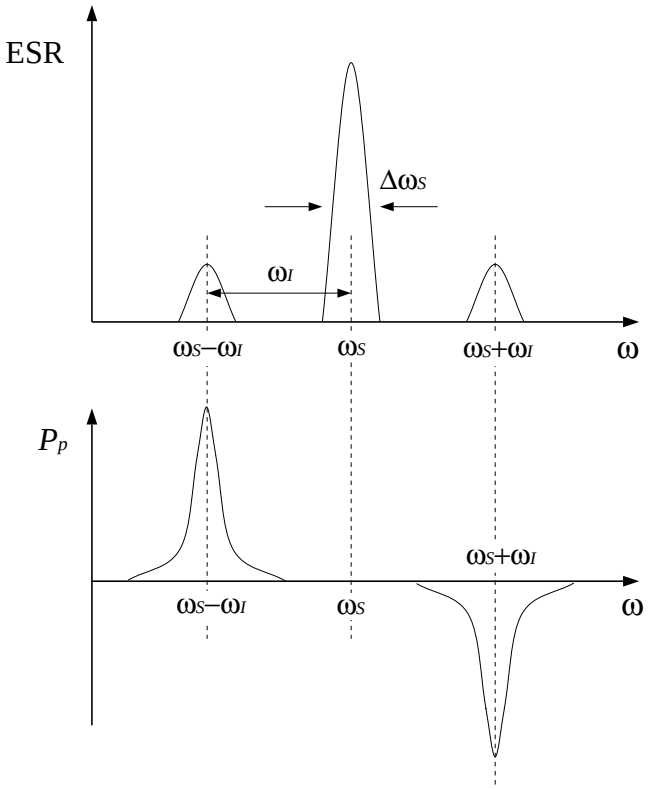

Figure 2.3: Schematic view of the ESR spectrum and the frequency dependence of the proton polarization P_p in applying the high magnetic field. (See the text.)

The high magnetic field is of importance for the solid effect. There are three transitions, $\omega = \omega_S - \omega_I$, $\omega = \omega_S$, $\omega = \omega_S + \omega_I$ which correspond to three peaks in the electron spin resonance(ESR) spectrum. If the linewidth $\Delta\omega_S$ is narrower than ω_I, the ESR spectrum is expected to the shape as shown schematically in Figure 2.3. Under the condition $\Delta\omega_S \lesssim \omega_I$, the electron polarization can be transferred to protons efficiently at $\omega = \omega_S - \omega_I$ or $\omega = \omega_S + \omega_I$. Since the typical value of $\Delta\omega_S$ is about 50MHz[3], the solid effect is effective at $H_0 \sim 25$ kGauss which gives $\omega_I \sim 105$ MHz.

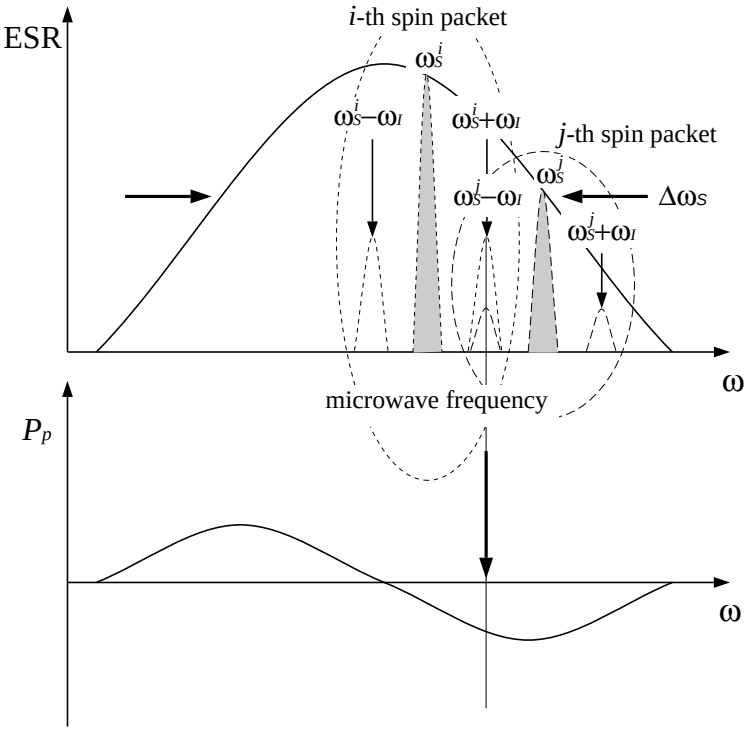

Figure 2.4: Schematic view of the ESR spectrum and the frequency dependence of the proton polarization P_p in the case of $\Delta\omega_S \gg \omega_I$. The parts shown by dotted lines are the ESR spectrum of the i-th spin packet, whereas the parts shown by dashed lines are that of the j-th spin packet. (See the text.)

In low magnetic field $\Delta\omega_S$ is wider than ω_I. In this case the ESR linewidth is assumed to be inhomogeneously broadened. It is the composition of spin ensembles which are homogeneously broadened as shown in Figure 2.4. They are called the spin packets. The i-th spin packet has the central resonance frequency of ${\omega_S}^i$ and the homogeneous broadening of ${\Delta\omega_S}^i$, in which ${\Delta\omega_S}^i \ll \omega_I$ is fulfilled. When the microwaves with the frequency $\omega(= \omega_S^i + \omega_I)$ are irradiated, the protons in the i-th spin packet are polarized in the $-$z direction, whereas the protons in the j-th spin packet, in which ${\omega_S}^j = \omega + \omega_I$, are polarized in the +z direction. The contribution of both spin packets to the proton polarization are canceled out each other. If we define

$h(\omega)$ as the magnitude of ESR line composed of narrow spin packets, the proton polarization P_p is proportional to the difference of $h(\omega - \omega_I)$ and $h(\omega + \omega_I)$ as

$$P_p \propto h(\omega - \omega_I) - h(\omega + \omega_I) \approx -2\omega_I \frac{dh(\omega)}{d\omega}, \qquad \text{if } \Delta\omega_S \gg \omega_I. \tag{2.9}$$

The microwave-frequency dependence of proton polarization is shown as the differential of the ESR spectrum(Figure 2.4). It is called the "differential solid effect". The cancelation among many spin packets gives rise to the inefficiency of the solid effect. For the efficient polarization transfer, the condition that $\Delta\omega_S$ is narrower than ω_I is required. It is fulfilled in high magnetic field.

2.2 Integrated solid effect

The integrated solid effect(ISE) is the method to polarize the proton efficiently by sweeping the frequency of microwaves in low magnetic field[32, 33]. In this case it is possible to transfer the polarization of electrons to protons efficiently, since the contributions of all the spin packets to the proton polarization are not canceled.

A spin packet in an ESR spectrum in an external magnetic field along the z-axis is considered. In applying the oscillating magnetic field $2H_1 \boldsymbol{e}_x \cos\omega t$ along the x-axis, which is perpendicular to the z-axis, an electron spin Hamiltonian $\boldsymbol{H}_S$ is given as

$$\boldsymbol{H}_S = \gamma_S H_0 S_z + 2\gamma_S H_1 S_x \cos\omega t, \tag{2.10}$$

where H_0 is the static external field. S_z and S_x show the z-component and the x-component of the electron spin vector, respectively. In the rotating frame x', y', z' with the frequency of ω around z-axis, the Hamiltonian is expressed as

$$\boldsymbol{H}_{rot} = (\omega_S - \omega) S_{z'} + \omega_R S_{x'}, \tag{2.11}$$

where ω_R is the Rabi frequency, $\omega_R = \gamma_S H_1$. It represents the Zeeman interaction of the spin with the effective field which is oriented to the direction determined by

the two components ω_R, and $\omega_S - \omega$ as shown in Figure 2.5. The effective Larmor frequency ω_{eff} in this effective field is given by

$$\omega_{eff} = \sqrt{(\omega_S - \omega)^2 + \omega_R{}^2}. \tag{2.12}$$

The effective field is expressed as $H_{eff} = \omega_{eff}/\gamma_S$. The polarization transfer from the

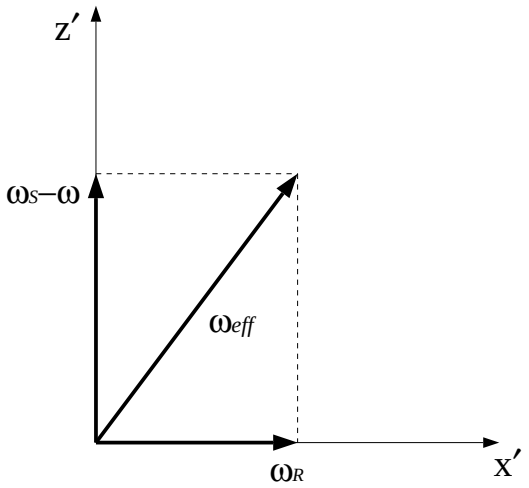

Figure 2.5: Effective field of the electron spin in the rotating frame

electron to the proton becomes most efficient in the case that the effective frequency ω_{eff} is equal to the Larmor frequency of proton ω_I[33, 40].

We consider that the external magnetic field H_0, or the frequency of irradiated microwave is swept through the resonance. When the external magnetic field changes adiabatically as shown in Figure 2.6(a), the direction of the electron spin vector changes following H_{eff} and finally it is reversed. The sweeping time is limited by the electron spin relaxation time. It is called the adiabatic fast passage. Here, at the points A and B where the condition $\omega_{eff} = \omega_I$ is fulfilled, the polarization transfer occurs(Figure2.6(b)). It is noticed that there is no cancelation of the polarization transfer at the points A and B, since the direction of an electron spin vector is always parallel to the effective field. If the external magnetic field is swept through the

resonances of all the spin packets over the linewidth of ESR spectrum, all the spin packets make the contribution to the polarization transfer as shown in Figure 2.7.

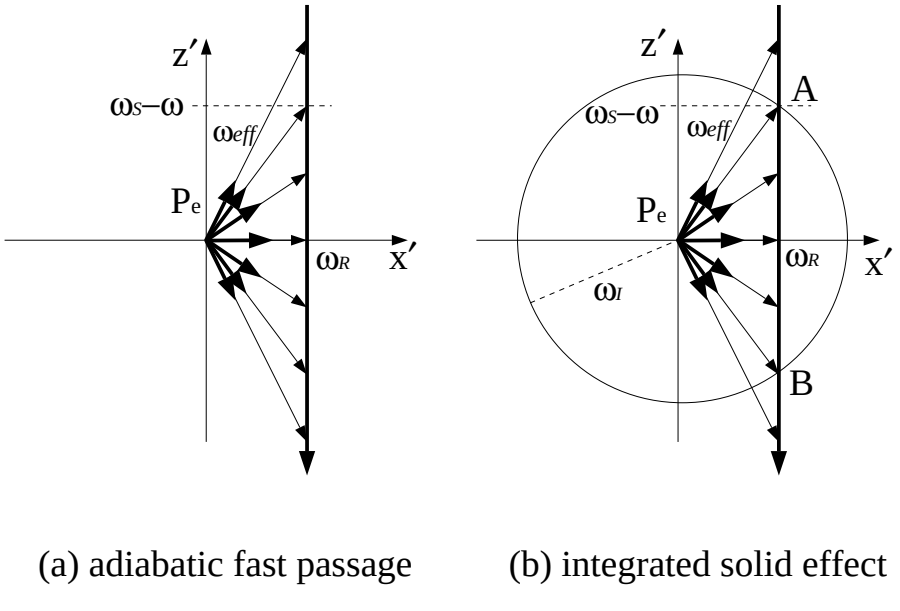

(a) adiabatic fast passage (b) integrated solid effect

Figure 2.6: Adiabatic fast passage and integrated solid effect in the rotating frame. (See the text.)

The adiabatic condition for reversal of the electron polarization vector is

$$\left|\frac{d\delta}{dt}\right| \ll {\omega_R}^2 \qquad \delta \equiv \omega_S - \omega. \tag{2.13}$$

In the case of sweeping the external field, the adiabatic condition is

$$\left|\frac{d\delta}{dt}\right| = \left|\frac{\omega_S}{dt}\right| = \left|\gamma_S \frac{dH_0}{dt}\right| \ll {\omega_R}^2. \tag{2.14}$$

Thus

$$\left|\frac{dH_0}{dt}\right| \ll \frac{{\omega_R}^2}{\gamma_S}. \tag{2.15}$$

In the case of sweeping the microwave frequency, the adiabatic condition is

$$\left|\frac{d\omega}{dt}\right| \ll {\omega_R}^2. \tag{2.16}$$

In addition, the condition

$$\omega_R \leq \omega_I \tag{2.17}$$

is also required. The polarization can be transferred from the electron to the proton in rather low magnetic field ($\leq$ 10kGauss) by means of the integrated solid effect under these conditions.

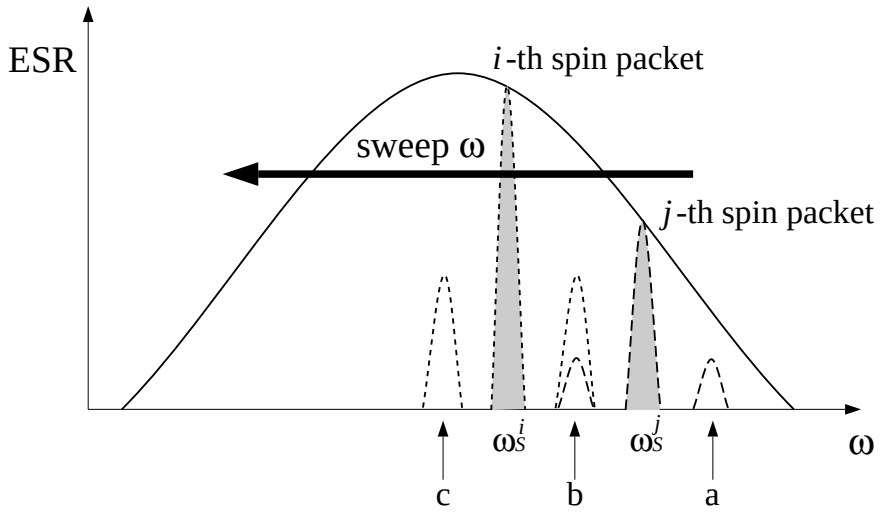

Figure 2.7: A schematic view of the integrated solid effect within the linewidth of the ESR-spectrum. 'a' corresponds to the point A of the j-th spin packet in Figure 2.6(b), 'b' to the point B of the j-th spin packet and the point A of the i-th spin packet. 'c' corresponds to the point B of the i-th spin packet. The frequency of the microwave is swept as shown by the arrow.

The first experiment by means of the integrated solid effect was carried out by Henstra, et al.[32]. They polarized ^{29}Si nucleus in the single crystal of silicon doped with boron in 2.64kGauss at 1.2K. It was reported that the polarization by the integrated solid effect is 21 times as high as that by the differential solid effect.

2.3 Triplet state of the aromatic molecule

The thermal electron polarization in low magnetic field at high temperature is too small to be applied to the dynamic polarization of protons. However, the population differences on the triplet state of aromatic molecules are applicable to the dynamical proton polarization[31, 34].

An example of the energy levels of aromatic molecules are shown schematically in Figure 2.8. The spin state of the ground state of such a molecule is singlet. The electron is spontaneously aligned on the lowest triplet state T_0. However, the probability of the direct excitation from the ground state S_0 to T_0 is extremely small. On the other hand, the molecule can be excited to higher singlet states by optical

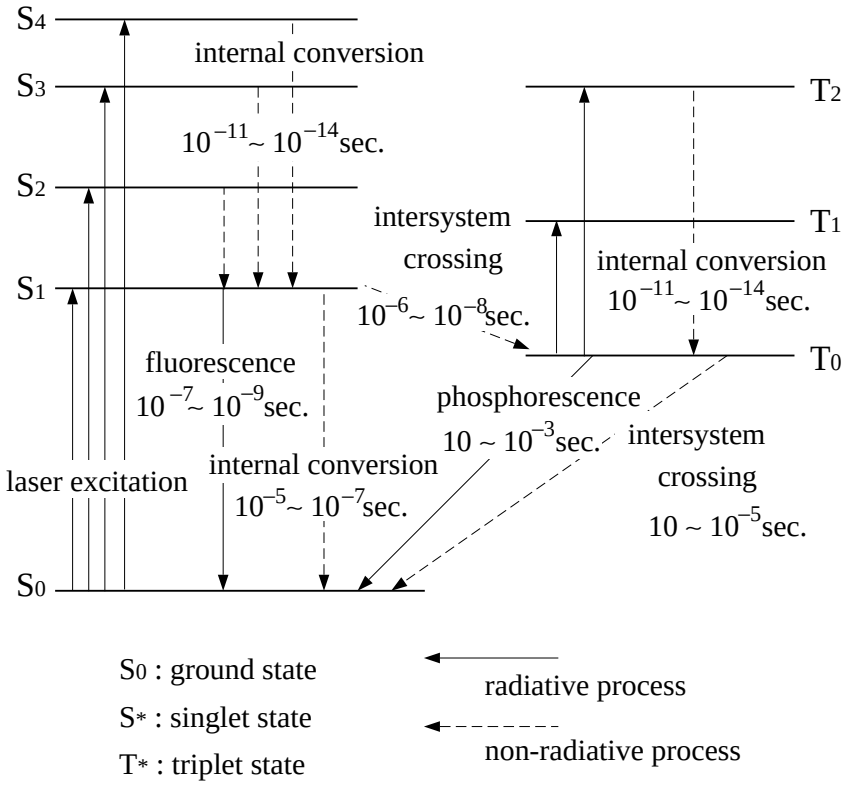

Figure 2.8: Typical energy levels of an aromatic molecule

pumping. It decays to the first excited singlet state S_1 very fast, typically within $10^{-11}\sim10^{-14}$ sec. due to the internal conversion, which is non-radiative transition between the same spin states. There are two possibilities of the transitions from the S_1 state, that is the decay to the ground state and the transition to the T_0 state due to the intersystem crossing. The intersystem crossing is a non-radiative process between different spin states caused by the spin-orbit interaction. There is a radiative decay process from the T_0 to the ground state, which is called the phosphorescence. Non-radiative decay due to intersystem crossing exists also. Radiative decay from the S_1 state to the ground state is known as the fluorescence, and non-radiative decay is due to the internal conversion. In addition, there is also the triplet-triplet transition from T_0 to higher excited triplet states by the absorption of photons. They decay to T_0 rapidly. The typical decay constants are also shown in Figure 2.8.

The transitions between the first excited singlet state and the sublevels of the triplet state are selective because the spin-orbit interaction causes the mixing only between the states with the same total symmetry[29, 35, 36]. Thus the alignment exists on the Zeeman sublevels of T_0. This population difference is almost independent of the temperature and the strength of the external field, but it depends on the direction of the external field. Therefore, single molecular crystal is indispensable as material for polarizing protons.

In order to obtain the high proton polarization in a low magnetic field at high temperature, the integrated solid effect is applied to the T_0 state within its lifetime. If the relaxation time of the electrons on T_0 is longer than the lifetime of the T_0 state, the relaxation among the Zeeman sublevels does not cause the relaxation of the proton spin substantially. The proton spin is kept polarized on the ground state for long time, since the state is diamagnetic.

2.4 Dynamic nuclear polarization on the photoexcited triplet state

2.4.1 Dynamic polarization of protons in the molecular crystal doped with pentacene molecule

The pentacene molecule $C_{22}H_{14}$ has a large population differences between the Zeeman sublevels of the triplet states. The populations of the Zeeman sublevels

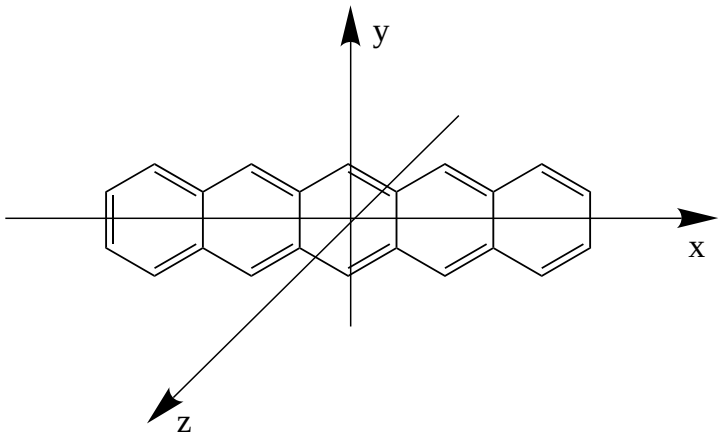

Figure 2.9: Molecular structure of the pentacene

$|+1>$, $|0>$ and $|-1>$ are 12, 76 and 12% respectively, when the external field is applied along the x-axis as shown in Figure 2.9[37].

It is known that naphthalene and p-terphenyl are suitable molecules for growing to single crystals doped with pentacene. A single crystal of naphthalene doped with pentacene is considered. The level diagram of the pentacene molecule is shown in Figure 2.10. In order to polarize the proton in the crystal dynamically, a pulsed laser beam is applied to the crystal, in which pentacene is excited to one of higher singlet states and then it decays into the lowest triplet state T_0. During the period when pentacene remains on the T_0 state, microwaves are irradiated while the external field is swept simultaneously for pursuing the dynamic proton polarization by means of

the integrated solid effect. Pentacene decays from the triplet state T_0 into the ground state with the decay constant of about 20μsec.[38]. As the excitation of the pentacene and the sequential ISE are repeated, the proton polarization increases. Since the

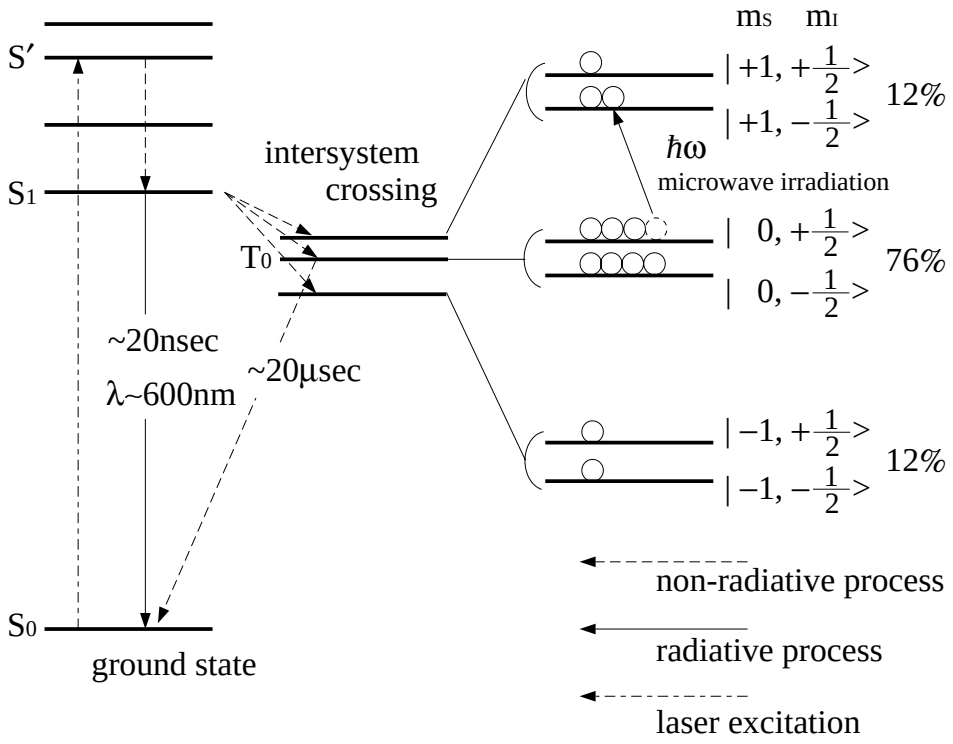

Figure 2.10: Energy levels of pentacene: The values on the right side represents the population differences of each sub-levels on T_0. The state S′ is one of higher singlet states than the state S_1.

electron spin-lattice relaxation time is longer than the decay time of T_0[40], it is expected that the influence of the electron spin relaxation to the proton spin is small. After the electron polarization is transferred to a proton in a pentacene molecule or to a proton in a naphthalene molecule near a pentacene by integrated solid effect, the polarization is diffused by the spin-spin interaction between proton spins. As the result, most of the protons in the naphthalene molecules are also polarized.

2.4.2 Buildup and relaxation of the polarization

The maximum proton polarization is determined by the balance between the buildup rate and the relaxation rate of the polarization. In general, the time evolution of the polarization is given as the phenomenological formula

$$\frac{dP_p}{dt} = A(P_e - P_p) - \Gamma(P_p - P_{pth}), \tag{2.18}$$

where P_p is the proton polarization, P_e the electron polarization, and P_{pth} the proton polarization in thermal equilibrium. A is the buildup rate of the polarization, and Γ the relaxation rate. In this formula it is shown that the proton polarization approaches the electron polarization P_e with the buildup rate A due to pumping with microwaves, whereas it has a tendency to decay spontaneously to the thermal polarization P_{pth} with the relaxation rate Γ. The following relations are derived from Equation (2.18).

$$P_p = P_{p0}(1 - \exp(-(A + \Gamma)t)), \tag{2.19}$$

where

$$P_{p0} = \frac{A}{A + \Gamma} P_e. \tag{2.20}$$

Here P_{pth} is neglected, since P_{pth} is quite small, that is 10^{-6} at room temperature in 3kGauss. For obtaining the high proton polarization, the buildup rate should be large, and the relaxation rate should be small. The buildup rate can be written as

$$A \propto C\alpha(\lambda)\frac{E}{S}\beta\varepsilon R, \tag{2.21}$$

where $\alpha(\lambda)$ is the absorption coefficient of the laser power in pentacene (λ is the wavelength of the laser.), R the repetition rate, ε the transfer rate of polarization from an electron to a proton for every sequence. C is the density of pentacene, β the transition rate from the first excited singlet state to the lowest triplet state, E the energy of the laser pulse, S the area of the laser beam on the crystal.

In the ISE method pentacene molecule on the lowest triplet state decays into the ground state during the sweep of the magnetic field. Therefore, the values of P_e and A which depend on the number of electrons decrease during this period. Equation (2.18) is rewritten approximately as the formula

$$\frac{dP_p}{dt} = \bar{A}(\bar{P}_e - P_p) - \Gamma(P_p - P_{pth}), \tag{2.22}$$

where $\bar{P}_e$ and $\bar{A}$ are the average values of P_e and A respectively. $\bar{P}_e$ and $\bar{A}$ are expressed as

$$\bar{P}_e = \frac{1}{\Delta t}\int_{\Delta t} P_e(t)dt, \tag{2.23}$$

$$\bar{A} = \frac{1}{\Delta t}\int_{\Delta t} A(t)dt \tag{2.24}$$

respectively, where Δt is the sweeping time. The value of $\bar{P}_e$ is obtained by the waveform analysis of the ESR signals.

Chapter 3

Experimental Procedure and Apparatus

3.1 Overview of experimental procedure

Protons in naphthalene and p-terphenyl doped with pentacene are polarized by repeating the following three steps.

1. Pentacene molecules are excited to the lowest triplet state through singlet excited states by means of laser excitation.

2. The population difference between two electron Zeeman sublevels on the lowest triplet state is transferred to the proton polarization by means of the integrated solid effect within the lifetime of the triplet state.

3. The transition from the triplet state of pentacene molecules to the diamagnetic ground state occurs spontaneously.

The polarization of protons is measured by the nuclear magnetic resonance (NMR) after performing the dynamic polarization.

The experimental setup was composed of pulsed laser systems, a magnet, a microwave system for the ISE and ESR detection, and a pulsed NMR system for mea-

suring the proton polarization.

In order to excite pentacene to the electronic levels, we used a high power dye-laser with the pulse width of about 800nsec. A pulsed N_2-laser with the wavelength of 337nm was also used for studying the properties of the triplet states.

The magnetic field for the ESR and the NMR was about 3kGauss.

The microwave system was used for the dynamic polarization by means of the ISE and for a CW ESR-spectrometer with the resonance frequency of about 9.3GHz. During the irradiation of the microwave power the external magnetic field was swept using an internal coil in a cylindrical cavity (TE011-mode, $Q \sim 6000$). The cavity was mounted at the central position between two pole pieces. In this cavity, the sample whose size was about 3mm×5mm×2mm was placed. The CW ESR spectrometer was used for detection of the population difference between the electron Zeeman sublevels of the lowest triplet state of pentacene molecules. By monitoring a linewidth and a magnitude of ESR spectrum, the long molecular axis of pentacene(x-axis as shown in Figure 2.9) in the sample was aligned parallel to the the external field. The sweeping range of the magnetic field for performing the ISE was determined by the linewidth of the ESR spectrum.

For the measurement of the proton polarization the pulsed NMR technique was utilized in which the free induction decay (FID) signals of protons were detected. We applied RF pulses with the frequencies of about 12.95MHz and the widths of about 1.8μsec for detecting the FID signals of protons in thermal equilibrium and also after the dynamic polarization in order to obtain the enhancement factor. The NMR coil was inserted in the cavity only when the FID signal was measured. When the experiment was carried out at liquid nitrogen temperature, the sample was placed in a dewar.

Before mounting the sample in the apparatus, the absorption spectra of light in naphthalene and p-terphenyl doped with pentacene were measured to determine the best wavelength of the pulsed laser for the excitation of pentacene. The crystals with good quality were selected by the measurement of the line shapes observed with the ESR detection system.

In order to obtain the buildup and the relaxation curves of the proton polarization as a function of time, the weak RF pulse, by which the polarization was not disturbed significantly, was applied. The relaxation time was also obtained by measuring the recovery time of the polarization from zero to the value according to the Boltzmann distribution by using the 90° RF pulse.

3.2 Sample

The properties of single crystals of naphthalene $C_{10}H_8$ and p-terphenyl $C_{18}H_{14}$ are presented in Table 3.1. Figure 3.1 shows the structures of both molecules. Af-

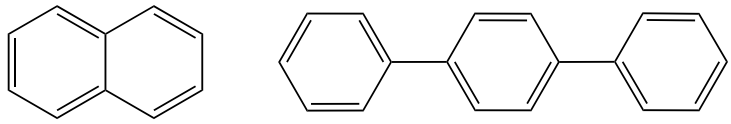

(a) naphthalene (b) p-terphenyl

Figure 3.1: Structures of the molecules of naphthalene and p-terphenyl

ter these molecules were purified by recrystalizaiton and zone melting, they grew to single crystals by the Bridgeman technique. In these molecules, the direction of crystal growth is on the b-axis shown in Figure 3.2 and Figure 3.3. Since the melting point of naphthalene and p-terphenyl are 80.55°C and 214°C respectively, it is not so difficult to obtain the single crystal growing in a glass tube. The crystal structures of naphthalene[41] and p-terphenyl[42] are shown in Figure 3.2 and Figure 3.3

respectively.

molecule	naphthalene	p-terphenyl
molecular formula	$C_{10}H_8$	$C_{18}H_{14}$
molecular weight	128.2 g/mol	230.3 g/mol
density	1.16 g/cm^{-3}	1.24 g/cm^{-3}
crystal structure	monoclinic	monoclinic(T>193K)*)
space group	$P2_1/a$	$P2_1/a$
a	8.2 Å	8.1 Å
b	6.0 Å	5.6 Å
c	8.7 Å	13.6 Å
α	90.0°	90.0°
β	123.0°	92.1°
γ	90.0°	90.0°
cleavage plane	ab	ab
number of unit cell	2	2
Reference	[41]	[42]
relaxation time of proton (at room temperature)	40min. (Ref. [33])	8min. (Ref. [44, 45, 46])

Table 3.1: Properties of the molecules of naphthalene and p-terphenyl. *)The crystal structure of p-terphenyl is triclinic($P\bar{1}$) at the temperature lower than 193K(Ref. [43]).

In naphthalene crystal, whose space group is $P2_1/a$, there are site A and site B. Two naphthalene molecules on site A or site B can be replaced with one pentacene molecule. The pentacene molecules on site A and site B are magnetically equivalent in the case that the external field is applied along the molecular x-axis[38]. It must

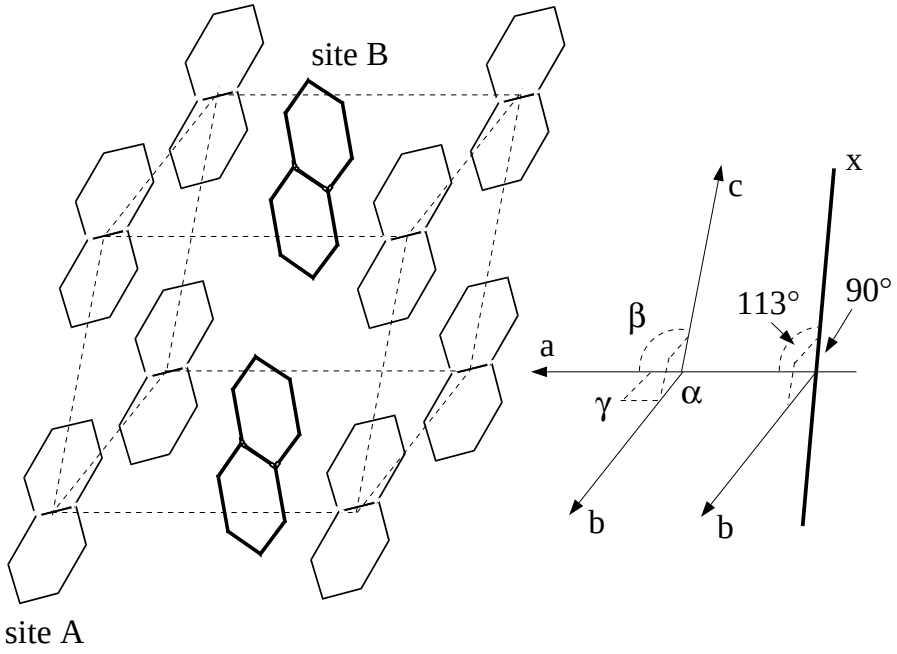

Figure 3.2: The crystal structure of naphthalene: The crystal is monoclinic and the space group is $P2_1/a$. The thin lines show the molecules on site A, and the thick lines show the molecules on site B. The x-axis is not parallel to the c-axis in the unit cell.

be noticed that the direction of the x-axis in pentacene is not parallel to the c-axis of a unit cell. The angle between the a-axis and the x-axis of pentacene is 113°, which is different from the angle β between the a-axis and the c-axis given in Figure 3.2[38].

The crystal structure of p-terphenyl crystal at the temperature higher than 193K is shown in Figure 3.3. The structure changes at 193K. In the crystal, whose space group is $P2_1/a$, there are site A and site B similar as naphthalene crystal. One p-terphenyl molecule on site A or site B is replaced with one pentacene molecule.

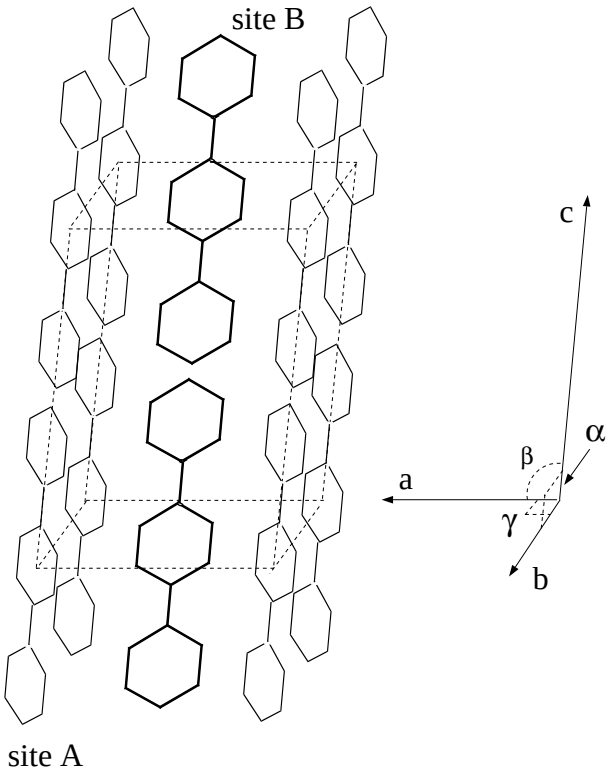

Figure 3.3: The crystal structure of p-terphenyl(T>193K): The crystal is monoclinic and the space group is $P2_1/a$. The thin lines show the molecules on site A and the thick lines show the molecules on site B.

Typical concentration of pentacene in naphthalene crystal is 0.01mol%, and that in p-terphenyl crystal is 0.1mol%. The p-terphenyl crystal has an advantage of the concentration of pentacene over the naphthalene crystal. However, the relaxation time of the proton spin in the naphthalene crystal is longer than that in the p-terphenyl crystal.

The absorption spectra in doped crystals were measured before DNP experiments. Typical absorption spectra in naphthalene and p-terphenyl crystals are shown in Figures 3.4 and 3.5. Since ultraviolet rays are absorbed in the host molecules at large absorption rates, it is not advantageous to use a laser beam with short wavelength for exciting only the pentacene molecules. The wavelength of the laser to excite the

pentacene molecule in naphthalene crystal most efficiently was found to be 595nm. For p-terphenyl crystal, the wavelength of 590nm was preferable. At liquid nitrogen temperature, the widths of the lines are narrower than those at room temperature. The dip position of the absorption curve for naphthalene crystal was found to be shifted from 595nm to 600nm at liquid nitrogen temperature. In the case of p-terphenyl, the shift of the dip position was negligibly small.

The dye-laser whose wavelength is approximately 600nm was found to be the most suitable for exciting pentacene molecules in both host crystals at liquid nitrogen temperature and room temperature. Another advantage of the dye-laser is in the fact that the wavelength is variable.

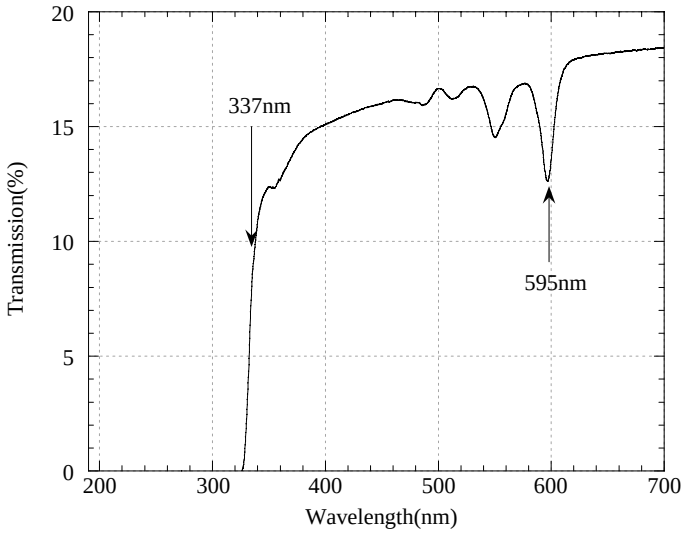

Figure 3.4: Absorption spectrum in a single crystal of naphthalene doped with pentacene at room temperature: The thickness of the crystal was 1.8 mm. The spectrum was obtained with the spectrophotometer(Shimadzu, MPS-2000).

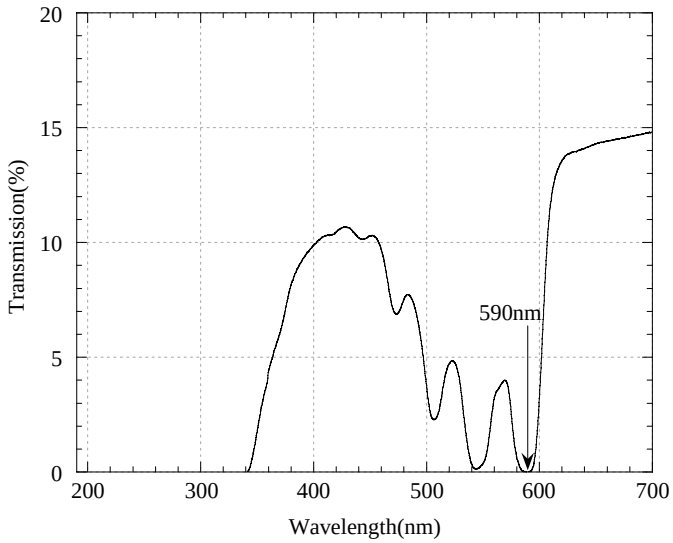

Figure 3.5: Absorption spectrum in a single crystal of p-terphenyl doped with pentacene at room temperature: The thickness of the crystal was 2.2 mm. The spectrum was obtained with the same equipment as the one in the case of naphthalene.

3.3 Experimental apparatus and their performance

3.3.1 Pulsed laser system

The pulsed laser is advantageous over the CW laser for polarizing protons in pentacene molecules efficiently, since the excitation of pentacene by the CW laser reduces the population difference between the Zeeman sublevels on the lowest triplet state. The populations of the Zeeman sublevels $|+1>$, $|0>$ and $|-1>$ in excitation of the CW laser, are calculated to be 30.6%, 38.8% and 30.6% respectively. Since the transition time from S_1 to T_0 is about 1μsec. which is longer than the transition time of S_1 to the ground state S_0($\sim$ 20nsec.)[39], the pulse width of the laser beam longer than the transition time to the ground state is preferable. Using such a laser beam, the excitation of pentacene can be repeated during one pulse. As a result, the population on T_0 including all the Zeeman sublevels is accumulated, if the energy of the laser pulse is sufficiently high. However, the pulse width should be less than 20μsec. because the decay time of T_0 to the ground state S_0 is about 20μsec. In excitation by the laser beam with the short pulse width, the population has the tendency to be saturated as the pulse energy of the laser beam increases. In this experiment, we used a pulsed dye-laser with a pulse width of about 800nsec. (Cynosure, model LFDL-3).

For studying the effect of the light absorption to excite from the lowest triplet state to higher triplet states, a pulsed N_2-laser(Lumonics Excimer laser, Series TE-860-4) was used. This laser could produce ultraviolet rays with the wavelength of 337nm. In the case of naphthalene, the total absorption rate of the N_2-laser is lower than that of the dye-laser, but the absorption rate on the triplet state is larger than the absorption rate of the dye-laser[47].

The specifications of the lasers are presented in Table 3.2.

	dye-laser	N_2-laser
wavelength	590nm~605nm	337nm
max. energy per pulse	10mJ	2mJ
max. repetition rate	50Hz	70Hz
max. average power	500mW	150mW
pulse duration	800nsec.	4nsec.
beam size	4mmϕ	10mm×20mm

Table 3.2: The specifications of the dye-laser and the N_2-laser

3.3.2 ESR system

Figure 3.6 shows the block diagram of the CW ESR system and ISE system. The solid lines in this diagram show the paths of the CW microwaves and the trigger pulses to the laser and to the oscilloscope for the ESR measurement. The dotted lines show the flows of the microwave pulse and the trigger pulse for the ISE. The double solid lines represent the waveguide.

ESR signals were observed as the decay of the population difference between two Zeeman sublevels as a function of time after irradiation of the pulsed laser beam. When the microwave power was filled in the cavity, the signal could be seen on a oscilloscope after a certain time from the trigger of the laser as shown in Figure 3.7.

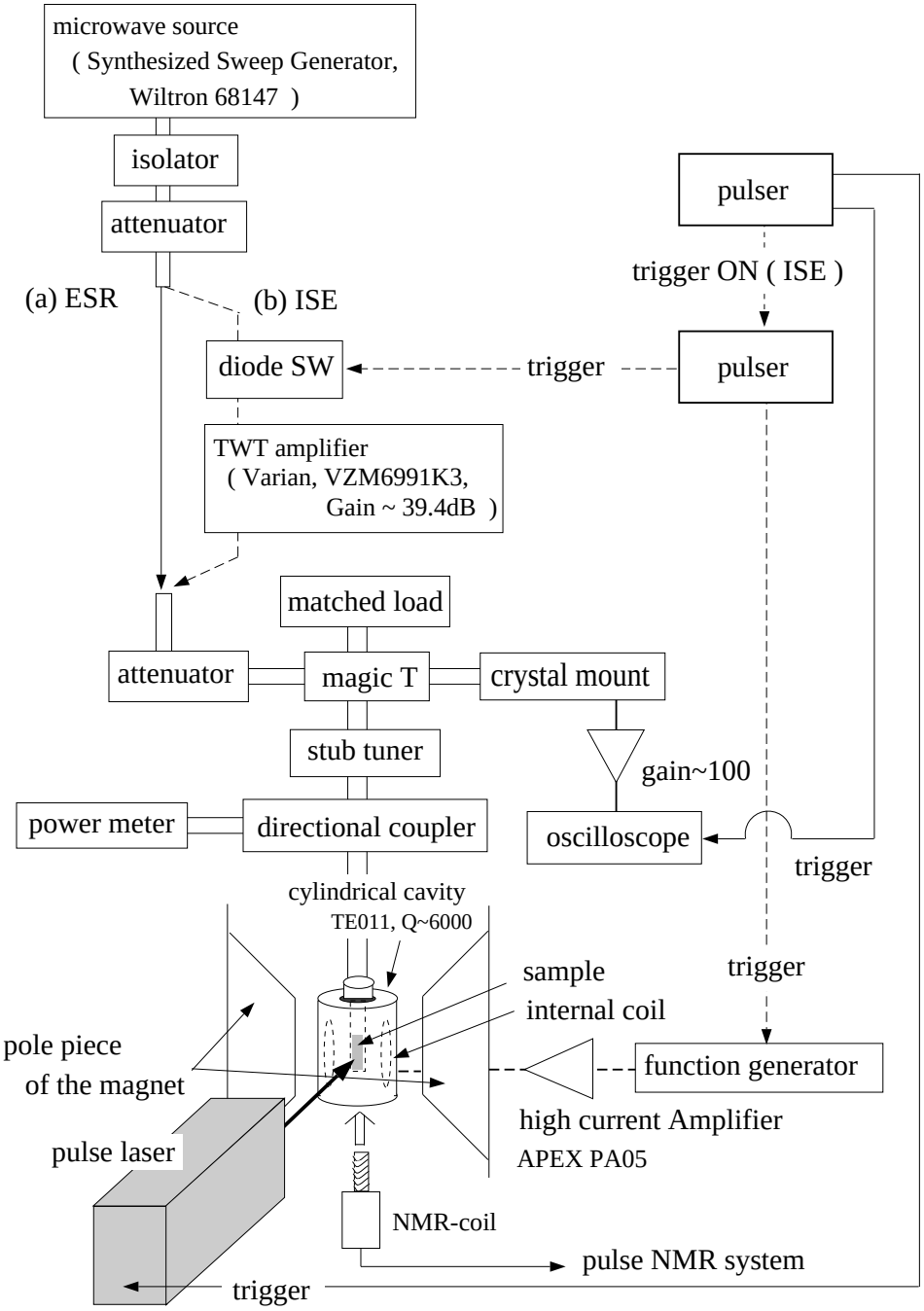

Figure 3.6: Block diagram of ESR system and ISE system: The solid lines show the paths of the CW microwaves and the trigger pulses to the laser and to the oscilloscope for the ESR measurement. The dotted lines show the flow of the microwave pulse and the trigger pulses for the ISE. The double solid lines represent the waveguide.

A synthesized sweep generator was used as the microwave source. The output power was 63mW and the frequency was tuned to the resonance frequency of the cavity. The resonance frequency was 9.3GHz without a sample in the cavity, but shifted slightly when the sample was mounted. Microwaves which were produced in

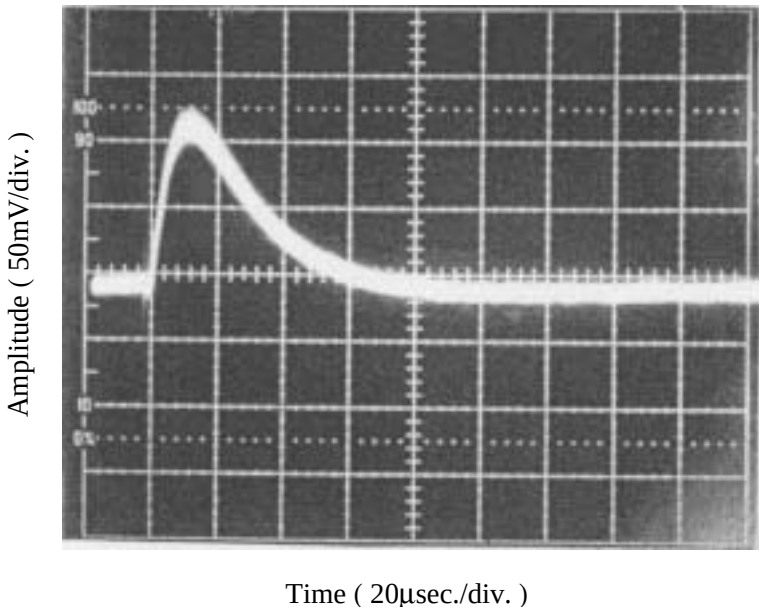

Figure 3.7: ESR signal shown in a oscilloscope

the microwave source passed through an isolator and an attenuator and then were split with a magic T. Outgoing microwaves from the magic T passed through a stub-tuner and then a directional-coupler. Finally, they reached the cylindrical cavity. The stub-tuner was used for impedance matching. Small part of the microwave power was extracted from the directional coupler to monitor the microwave power. Reflected microwaves from the cavity came back to the magic T, and were detected with a crystal diode.

DPPH(diphenylpicrylhiydrazyl) was used as a standard sample in order to tune the ESR system. After the direction of the x-axis of pentacene molecule was aligned

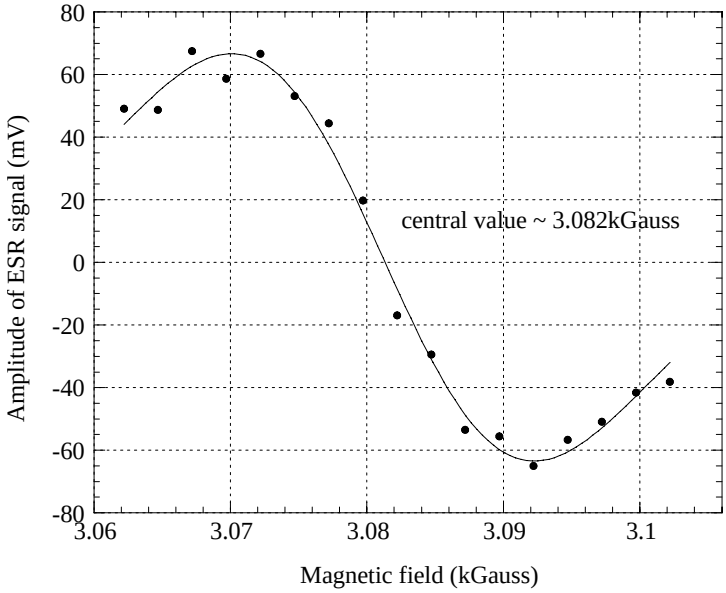

Figure 3.8: The ESR amplitude as a function of the magnetic field. The solid line is the curve fitted with the differentiated Gaussian function. The central magnetic field was 3.082kGauss.

parallel to the direction of the external field by monitoring the ESR signal, an ESR spectrum were obtained by changing the external magnetic field. Figure 3.8 shows the amplitudes of ESR signals as a function of the magnetic field. The solid line represents a curve fitted with the differentiated Gaussian function. Before performing the ISE, the external field was adjusted to the central value of the curve.

3.3.3 ISE system

The ISE system consisted of an internal coil in the cavity and a controller of irradiation of pulsed microwaves. Dotted lines in Figure 3.6 show the flows of the microwave pulse and the trigger pulses. The CW microwaves were pulsed with a diode switch. The pulse width was longer than 10μsec. Then they were amplified

by a TWT power amplifier with the gain of 39.4dB. A typical power of the pulsed microwaves was about 30mW.

The magnetic field was swept with the internal coil in the cavity. The sweeping current was made by amplifying the triangular wave produced in a function generator with a high power operational amplifier APEX-PA05. The maximum output current

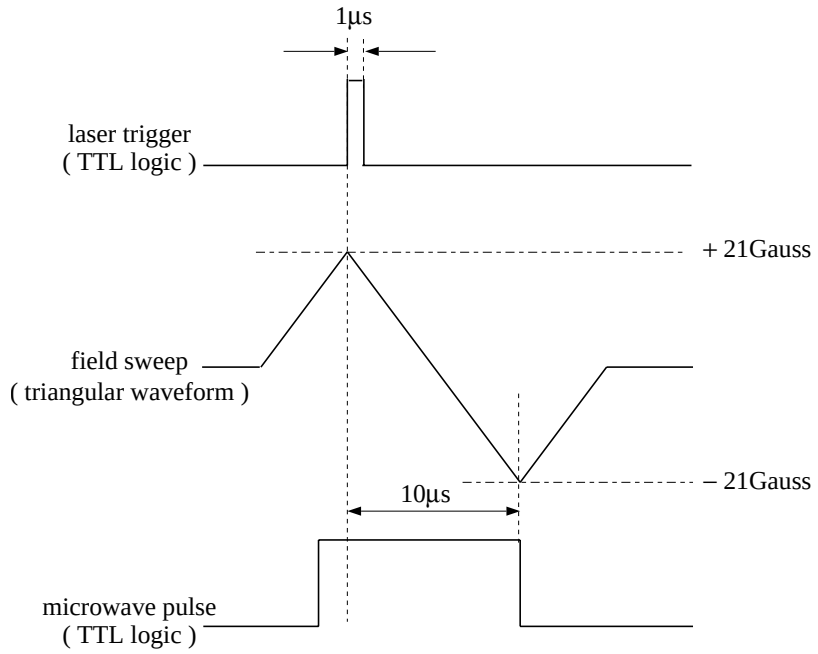

Figure 3.9: Time sequence of the pulses for the ISE

of the amplifier is ±30A and the slew rate is 100V/μsec. In fact, the sweep current was set to ±25A, which corresponded to ±21Gauss. It was sufficient for performing the ISE. These apparatus and the laser system were synchronized with the trigger pulse. The width of field sweep was about 10μsec. The time sequence is shown in Figure 3.9.

3.3.4 NMR system

After the dynamic nuclear polarization was performed by means of the ISE, the proton polarization was measured with a pulsed NMR system, in which the response of the magnetism was observed. The block diagram of the pulse NMR system is shown in Figure 3.10.

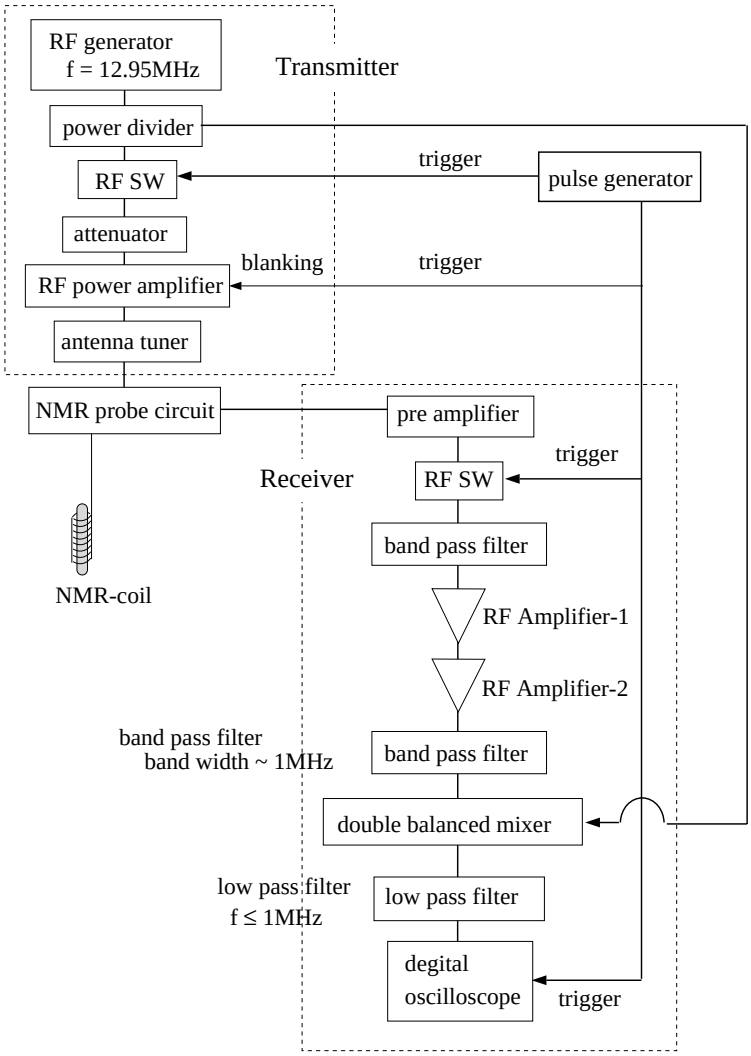

Figure 3.10: Block diagram of the NMR system

The NMR system was composed of a transmitter, a probe, and a receiver. The

RF pulse was created in a CW RF-generator and a RF switch. The RF pulse of 3mW was amplified with a high power amplifier which had a gain of 57dB. The maximum output power was 500W. The output of the high power amplifier was blocked by the "blanking" pulse when the receiver was active, since it gave rise to the noise in the receiver. The frequency of the RF pulse was 12.95MHz, and the power was adjusted

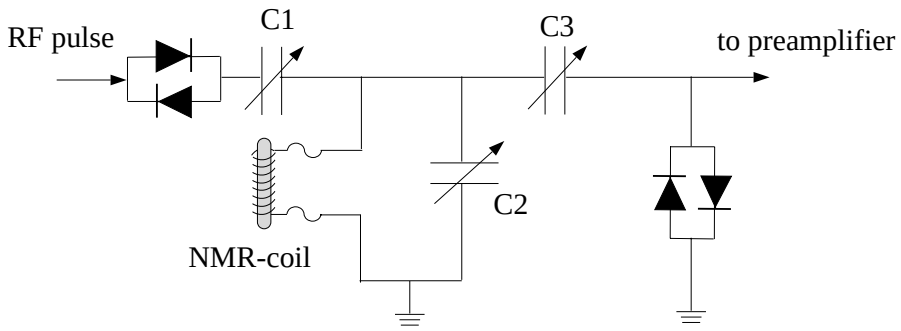

Figure 3.11: NMR probe circuit. C1∼C3 are the capacitors.

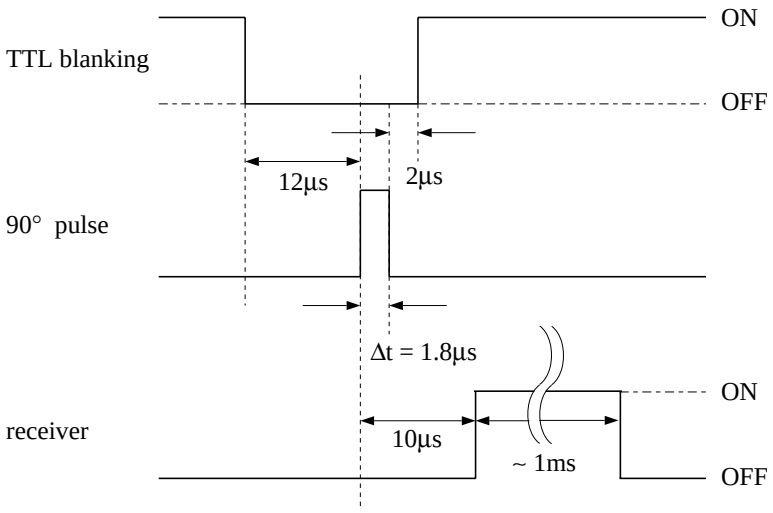

Figure 3.12: Time sequence of the pulses in the NMR system

with attenuators inserted just before the RF power amplifier. The pulse width of

the 90° pulse for the free induction decay was adjusted to be 1.8μsec. The 90°pulse was transmitted to the NMR probe circuit through an antenna tuner for impedance matching. Figure 3.11 shows the circuit for the NMR probe. After the 90° pulse was applied to the sample with a parallel LC resonant circuit, the FID signals were picked up with the same LC circuit. The receiver circuit was switched on 10μsec after the 90° pulse started in order to eliminate the disturbance of the signal by the 90° pulse. The time sequence among the operation of the receiver, the applying RF pulse and the blanking pulse is shown in Figure 3.12. The signal of 12.95MHz including the FID was extracted through the amplifiers and band-pass filters. The FID signal was detected as a phase sensitive signal with a double balanced mixer and observed on a digital oscilloscope.

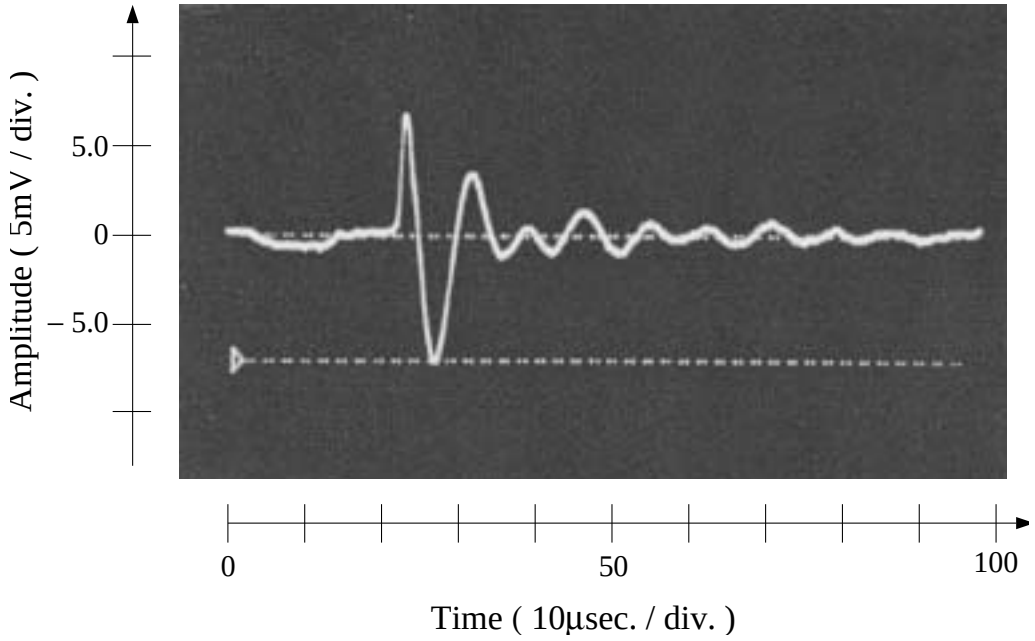

Figure 3.13: A FID signal on the oscilloscope

A typical FID signal observed with this system is shown in Figure 3.13. Since the external field was different slightly from the resonance field for the proton spin, a beat between the Larmor frequency and the applied RF frequency was observed in

the picture. The amplitude of FID just after applying the 90° pulse(t=0) corresponds to the area of NMR spectrum, which is proportional to the proton polarization. In order to obtain the absolute value of the polarization, we detected the FID signal in the thermal equilibrium. The comparison of the enhanced signal with the signal in the thermal equilibrium could be done without complicated shape analysis, since the shape of the both FID signals were similar even the sizes were so much different.

Figure 3.14 shows the linearity of the output voltage detected with the receiver versus input RF voltage. The RF power was supplied to an auxiliary coil near the NMR pickup coil. The horizontal axis represents the voltage of RF applied to the auxiliary coil. The vertical axis shows the output voltage observed with the receiver

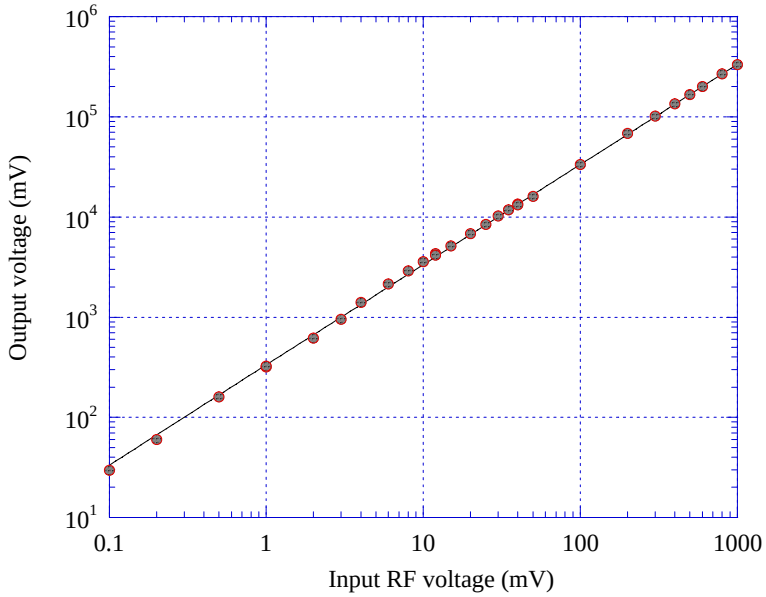

Figure 3.14: Linearity test of NMR coil. The output voltage detected with the receiver as a function of the input RF voltage supplied to the auxiliary coil.

just before the double balanced mixer. It is shown in Figure 3.14 that the dynamic range for the measurement of FID signals is about 10^4. When the 90° pulse was replaced by a weak RF pulse, the dynamic range of 10^4 could be covered. Therefore,

the signal enhancement higher than 10^4 could be detected using both the 90° pulse and the weak RF pulse. Signals measured with the weak RF pulse were calibrated by the signals measured with the 90° pulse when the polarization of proton was about 0.1%. When the weak RF pulse is applied instead of the 90° pulse, the diminution of the polarization due to the NMR measurement is much less, even though the sensitivity of the NMR was smaller.

The thermal equilibrium signal was measured with the 90° pulse because the signal was very small. The measurement was carried out in 5kGauss instead of 3kGauss, because the S/N ratio in 5kGauss was 1.6 times as high as that in 3kGauss. Since the relaxation time of proton in naphthalene was about 2 hours in 5kGauss at room temperature, we waited for about 10 hours before the measurement of the signal in the thermal equilibrium. In the case of p-terphenyl, we waited for about 1 hour since the relaxation time was about 10 minutes. When the dynamic polarization was carried out at liquid nitrogen temperature, we kept the sample in 5kGauss at room temperature during the waiting time, and then it was immersed in liquid nitrogen just before the measurement of the thermal equilibrium signal, because the relaxation time of proton spin was extremely long at liquid nitrogen temperature.

In order to obtain the buildup time of the proton polarization, we measured the increase of the FID amplitude with the weak RF pulse during the dynamic polarization. The relaxation time T_{1p} of the proton polarization is measured by two methods. One of them is to measure the decrease of the FID amplitude using the weak RF pulse after performing the dynamic polarization. The other one is the "saturation recovery method", in which the recovery time of the polarization from zero to the value corresponding to the Boltzmann distribution is measured using the 90° pulse.

Chapter 4

Experimental Results and Discussion on Dynamic Polarization

The experimental results on the polarization of protons in the naphthalene and p-terphenyl crystals doped with pentacene are presented and discussed. The population difference between the Zeeman sublevels on the triplet state of the pentacene molecule which is excited with the dye-laser is transferred to the proton polarization by means of the integrated solid effect. Then the pentacene molecules decay to the ground state. After this cycle is repeated many times, protons in the crystal are polarized substantially.

The experiments were carried out in the magnetic field of 3kGauss at room temperature and liquid nitrogen temperature.

4.1 Measurement of the population difference between the Zeeman sublevels

Waveform analysis of the ESR signal

The pentacene molecules were excited to the lowest triplet levels by means of optical pumping through singlet excited states using a pulsed laser. We used the pulsed dye-laser whose wavelength was adjusted to 595nm. The sample was a single crystal of naphthalene doped with 0.01mol% pentacene. The size of the crystal was 4.9mm×3.7mm×2.6mm. We carried out the experiment at room temperature.

The electron spin in the lowest triplet state is spontaneously aligned. If the x-axis of pentacene molecule is adjusted to be parallel to the external field, the populations of the Zeeman sublevels $|+1>$, $|0>$ and $|-1>$ are 12, 76 and 12% respectively, which are almost independent of the external magnetic field. The population differences between the sublevels were derived from the analysis of the time evolution of the ESR amplitude, of which picture on the oscilloscope is shown in Figure 3.7. The time evolution of the ESR amplitude averaged over the observations for 50 times in 3kGauss at room temperature is shown in Figure 4.1.

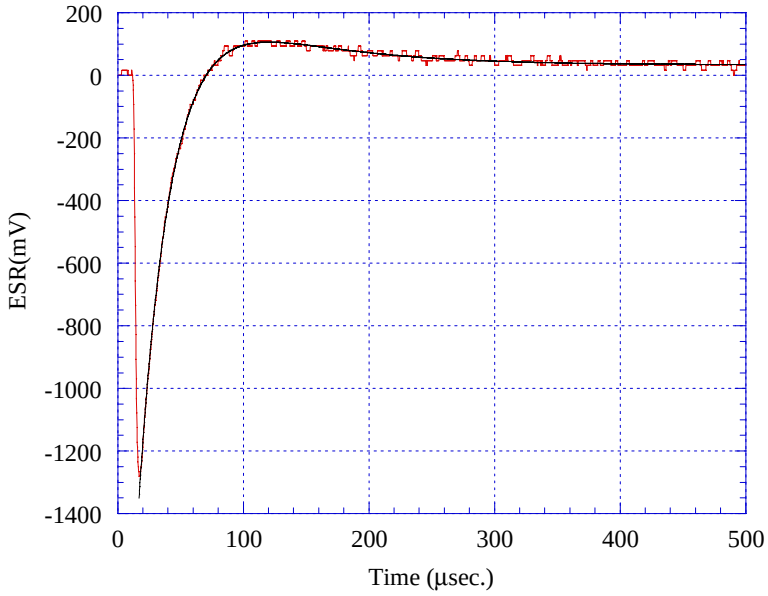

Figure 4.1: An ESR amplitude as a function of time for the transition between the sublevels $|-1>$ and $|0>$ of the triplet states of the pentacene in naphthalene crystal excited by the dye-laser. The experimental data averaged over 50 observations are shown. The energy of the laser pulse was 5mJ and the wavelength was 595nm(see the text). The data are fitted to the Equation (4.1) with the parameters k_1=0.012024μsec^{-1}, k_2=0.038306μsec^{-1} and m=0.1356, which is shown as the solid line.

The time dependent ESR amplitude shows the evolution of the transition between the states $|-1>$ and $|0>$, which corresponds to the population difference between these levels. The waveform is fitted to the formula

$$f(t) = \alpha((1-2m)e^{-k_2 t} - me^{-k_1 t}) + \beta, \tag{4.1}$$

where k_1 and k_2 are the transition rates from the states $|-1\rangle$ and $|0\rangle$ to the ground state respectively. The transition rates among three Zeeman sublevels on the triplet states are ignored in this equation, since these transition rates are much smaller than the transition rates to the ground state. The parameter m is the population of $|-1\rangle$ at the time when irradiation of a laser pulse was started(t=0). The populations of the sublevels, $|+1\rangle$, $|0\rangle$, and $|-1\rangle$ at t=0 are defined as $n_0(|+1\rangle)$, $n_0(|0\rangle)$, $n_0(|-1\rangle)$. They satisfy the relations

$$n_0(|+1\rangle) = n_0(|-1\rangle) = m, \tag{4.2}$$

$$n_0(|+1\rangle) + n_0(|0\rangle) + n_0(|-1\rangle) = 1. \tag{4.3}$$

The parameter α in Equation (4.1) is a scaling factor, and β is an offset. The solid line in Figure 4.1 represents the result of fitting, in which $k_1 = 0.012024\mu\text{sec.}^{-1}$, $k_2 = 0.038306\ \mu\text{sec.}^{-1}$ and $m = 0.1356$ respectively. The decay time constants of the states $|-1\rangle$, $|0\rangle$ are $\tau_1 = 1/k_1 = 83.2\mu$sec. and $\tau_2 = 1/k_2 = 26.1\mu$sec. respectively. Here, we define the 'electron polarization' as

$$P_e(t) = \frac{n(|0\rangle) - n(|-1\rangle)}{n(|0\rangle) + n(|-1\rangle)}, \tag{4.4}$$

where $n(|0\rangle)$ and $n(|-1\rangle)$ are the populations of the levels $|0\rangle$ and $|-1\rangle$ respectively. In this definition, we take into account the population difference only between two particular levels among three sublevels of the triplet state. The 'electron polarization' at t=0 $P_e(0)$ is described by the following expression with the parameter m

$$P_e(0) = \frac{n_0(|0\rangle) - n_0(|-1\rangle)}{n_0(|0\rangle) + n_0(|-1\rangle)} = \frac{1-3m}{1-m}. \tag{4.5}$$

$P_e(0)$ was 68.6% in the case shown in Figure 4.1. The linewidth of the ESR spectrum was about 22Gauss as shown in Figure 3.8.

The ESR amplitude is shown as a function of the laser energy in Figure 4.2, and $P_e(0)$ as a function of the laser energy in Figure 4.3. The beam size at the position of the sample was 8mmϕ. The points in both figures which corresponded to the same laser energy were derived from the same ESR signal. The ESR amplitude is proportional to the number of the excited pentacene, if the angle between the x-axis of pentacene molecule and the direction of the external field does not change. The ESR amplitude trends to be saturated when the laser energy increases. The average value of $P_e(0)$ was 71.1% which is close to the ideal value, that is 73%. $P_e(0)$ was

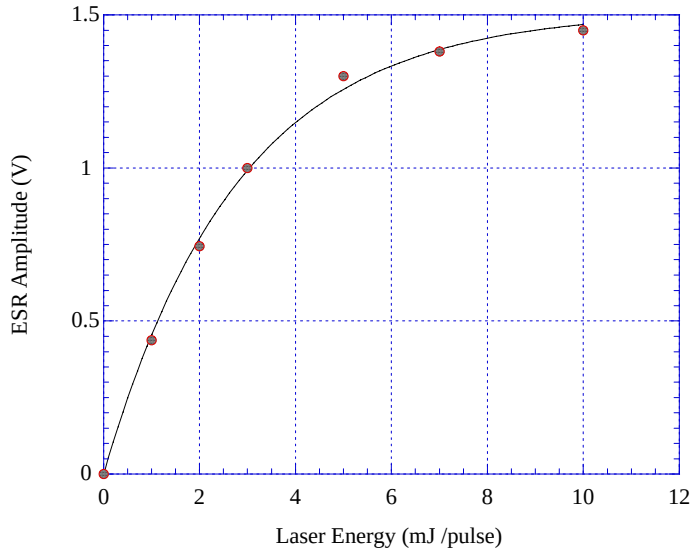

Figure 4.2: The ESR amplitude as a function of the laser energy. The size of laser beam at the position of the sample was 8mmϕ. The data were fitted to the exponential curve shown as the solid line.

found to be independent of the laser energy.

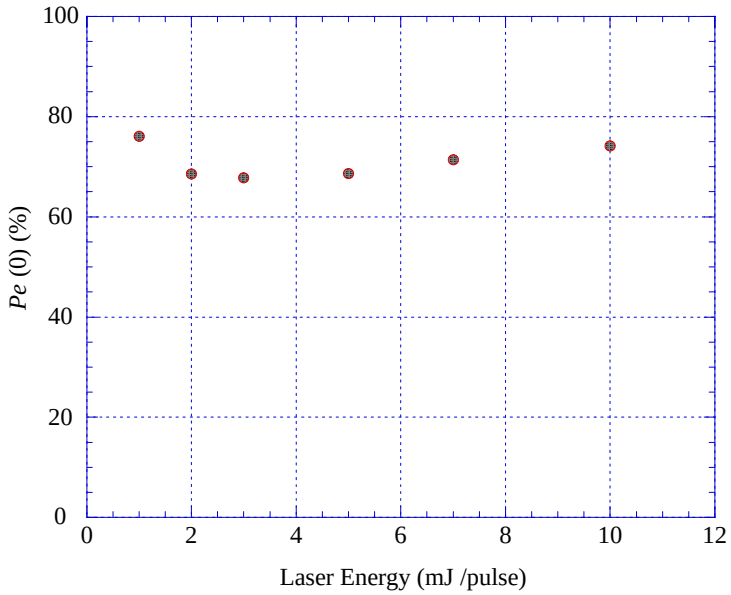

Figure 4.3: The 'electron polarization' $P_e(0)$ as a function of laser energy. The $P_e(0)$ was derived from the line shape of the ESR signal. The average value of $P_e(0)$ was 71.1%.

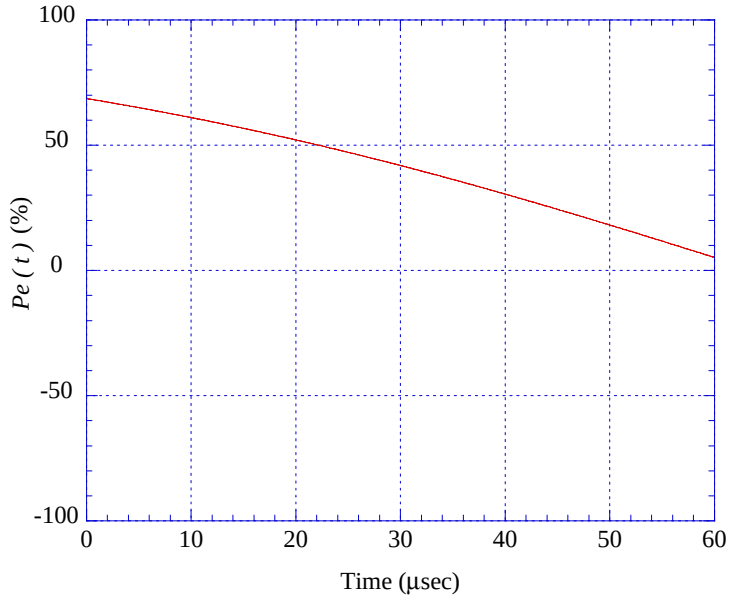

Figure 4.4: 'Electron polarization' as a function of time, where k_1=0.012024μsec.$^{-1}$, k_2=0.038306μsec.$^{-1}$ and m=0.1356 (See Equation (4.6).)

By using parameters k_1, k_2 and m, the 'electron polarization' $P_e(t)$ is expressed as

$$P_e(t) = \frac{(1-2m)e^{-k_2 t} - me^{-k_1 t}}{(1-2m)e^{-k_2 t} + me^{-k_1 t}}. \tag{4.6}$$

$P_e(t)$ is shown as a function of time in Figure 4.4, where t=0 is the time when the laser pulse is applied. The 'electron polarization' $P_e(t)$ decreases with time.

Study of triplet-triplet absorption

It was pointed out that if pentacene molecules are irradiated with a laser beam whose wavelength is shorter than 550nm, the excitation of higher triplet states, namely the triplet-triplet absorption(t-t absorption) process, occurs[48]. When a

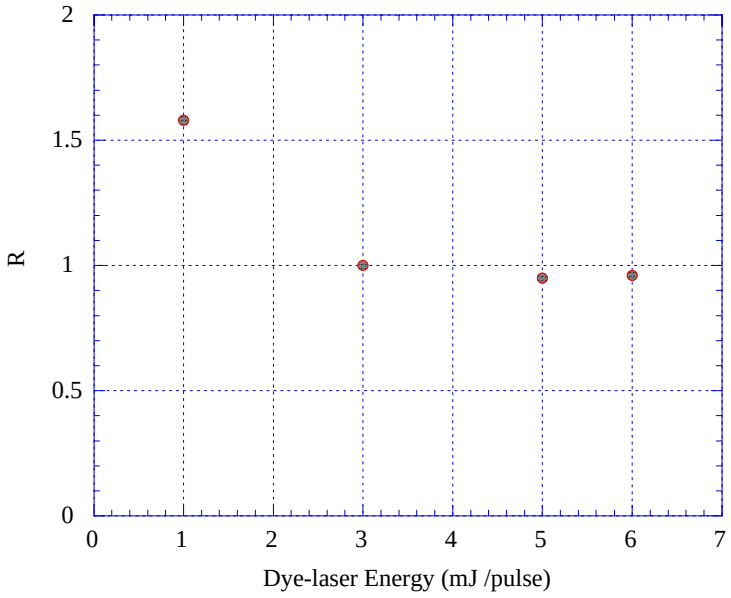

Figure 4.5: The ratio R of the ESR amplitudes in irradiation with the dye-laser and the N_2-laser to those only with the dye-laser are plotted as a function of the energy of the dye-laser. The energy of the N_2-laser is 2mJ.

crystal of a pentacene is irradiated with a N_2-laser beam of wavelength of 337nm, we can examine whether the triplet-triplet transition from the lowest triplet state to

the higher triplet state occurs. There is the possibility that the population difference between the Zeeman sublevels of the lowest triplet state T_0 changes by the t-t absorption.

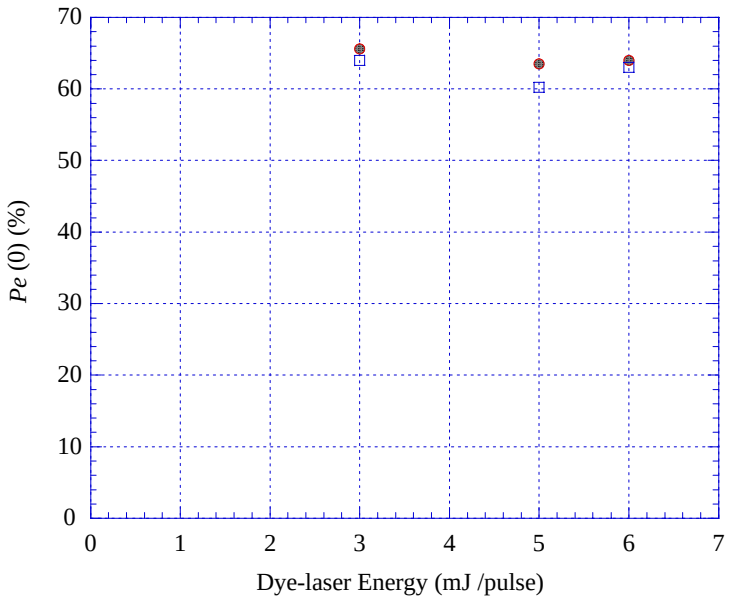

Figure 4.6: The 'electron polarization' $P_e(0)$ obtained by the waveform analysis as a function of the energy of the dye-laser. The solid circles show the results of the dye-laser irradiation. The open squares show the results of irradiation of the N_2-laser as well as the dye-laser. The energy of the N_2-laser is 2mJ.

In order to study the process, the crystal was irradiated with the pulsed N_2-laser just after pentacene molecules were excited to the lowest triplet state by the pulsed dye-laser irradiation. The ESR amplitudes in irradiation with both the dye-laser and the N_2-laser were compared to those only with the dye-laser. First, the ESR amplitude was measured as a function of the pulse energy of the dye-laser beam. The ESR amplitude was saturated at the energy higher than 5mJ per pulse as shown in Figure 4.2. Then the crystal was irradiated with both dye-laser and N_2-laser. As the pulse width of the dye-laser was about 800nsec, the irradiation of N_2-laser was delayed from the dye-laser irradiation by 1μsec. The ratio R of the ESR amplitudes

in irradiation with the dye-laser and the N_2-laser to those only with the dye-laser are plotted as a function of the pulse energy of the dye-laser in Figure 4.5. The energy of the N_2-laser is 2mJ. The size of the N_2-laser beam is 9mm×14mm at the position of the sample. The ratio R was larger than unity when the pulse energy of dye-laser was 1mJ, since the absorption of dye-laser was not saturated. On the other hand, R was almost unity when the energy of dye-laser was larger than 3mJ. Figure 4.6 shows $P_e(0)$ obtained by the waveform analysis of ESR signals as a function of the pulse energy of the dye-laser. It seems that $P_e(0)$ did not change much by N_2-laser irradiation. Therefore, it is expected that the t-t absorption does not cause the change of the population difference on the triplet state even if the t-t absorption occurs. However, there is indirect evidence of the t-t absorption as mentioned in 4.3.

4.2 Polarization transfer

The 'electron polarization' on the lowest triplet states can be transferred to the proton polarization by means of the integrated solid effect(ISE) as explained in Chapter 2. In order to transfer the polarization by the ISE, the magnetic field must be swept during the irradiation of microwaves as described in Subsection 3.3.3. The average 'electron polarization' $\bar{P}_e$ which is defined in Equation(2.23) decreases with the width of the field sweep Δt_{sweep}. Since the measured decay constant of the state $|0\rangle$ was about 26.1μsec. as presented in Section 4.1, Δt_{sweep} was set to be 10μsec. The input power of the microwaves P_{RF} was optimized to perform the polarization transfer most efficiently. In this experiment, P_{RF} were adjusted to be about 30mW, whereas the sweep width of the magnetic field ΔH_0 was set to be 42Gauss. It was confirmed that Equations (2.15) and (2.17) are fulfilled with these parameters.

The polarization of protons was measured by the NMR method shown in Subsec-

tion 3.3.4. First, we tried to confirm that the integrated solid effect was really effective at room temperature. For this purpose, the NMR signal was measured 1.5minutes after the irradiation of the pulsed N_2-laser with 50Hz and 25mW for 5minutes. The amplitude of the FID signal was proportional to the buildup rate, since the relaxation time is longer than polarizing time. The DNP was carried out with a single crystal of naphthalene doped with 0.01mol% pentacene in 3kGauss at room temperature.

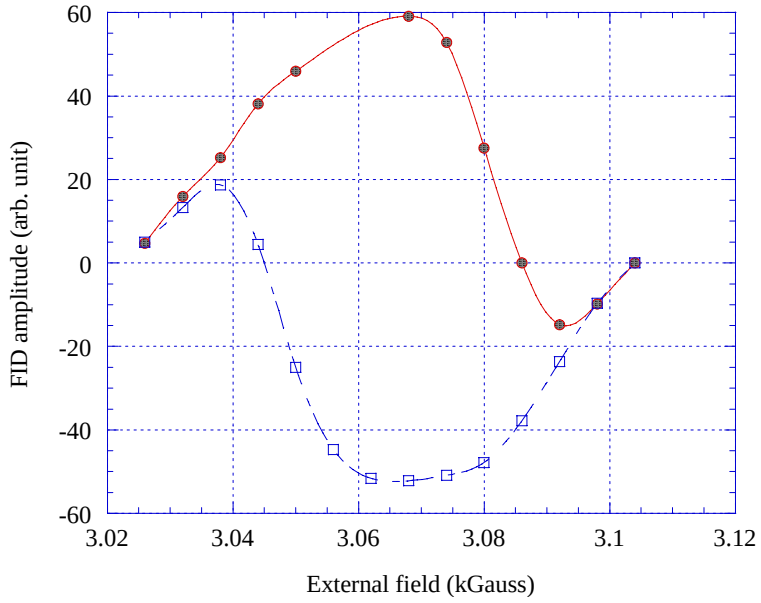

Figure 4.7: The amplitude of the FID signal as a function of the central value of the sweeping magnetic field where Δt_{RF} is 10μsec. The open squares give the amplitudes obtained when the external field was swept from higher value to lower value during the microwave irradiation, whereas the solid circles show those when the field was swept in the opposite direction.

Figure 4.7 shows the FID amplitude as a function of the central value of the sweeping magnetic field in the case that Δt_{RF} was 10μsec. and the sweep duration was 10μsec. The open squares give the amplitudes obtained when the external field was swept from higher value to lower value during the microwave irradiation, as shown in Figure 3.9, whereas the solid circles show those when the field was swept in the opposite direction. The sign of the polarization was reversed when the direction of

the field sweep was reversed. From the result we can conclude that the ISE is effective in this procedure.

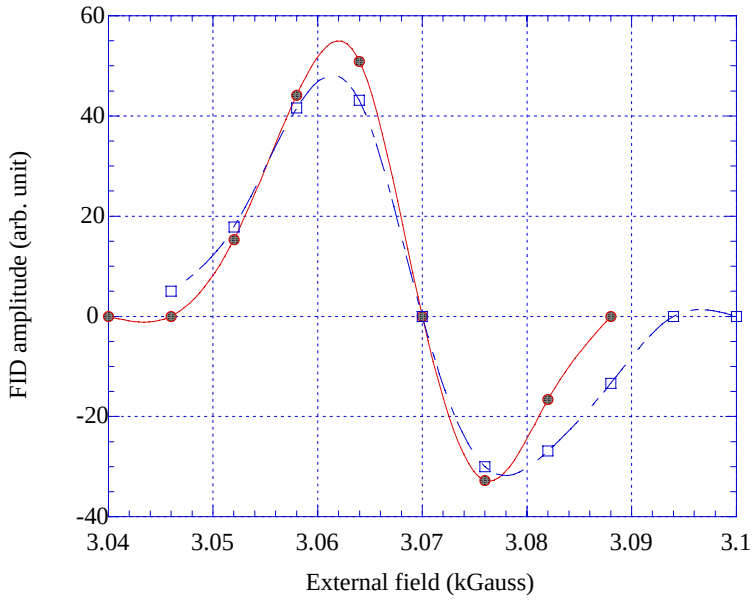

Figure 4.8: The amplitude of the FID signal as a function of the central value of the sweeping magnetic field where Δt_{RF} is 1μsec. and the sweeping time of the field was 10μsec. The open squares show the amplitudes obtained when the external field was swept from higher value to lower value during the microwave irradiation, whereas the solid circles show those when the field was swept in the opposite direction.

The FID amplitude versus the central field is shown in Figure 4.8, where the pulse width of microwaves Δt_{RF} was tuned to be 1μsec, while the sweeping time of the field was 10μsec. In this figure it is shown that the direction of the proton polarization is determined by the central field but not by the direction of the field sweep. The behavior is similar to the differential solid effect. The FID amplitude which corresponds to the proton polarization in these conditions was 10^{-1} times as large as the one with the long pulse width of microwaves. In these conditions, the width of the field sweep ΔH during the microwave irradiation was about 4.2Gauss, whereas the Zeeman splitting of the proton spin packet in the ESR spectrum was about 4.6Gauss.

4.3 Relaxation process

Naphthalene crystal

The relaxation process is usually considered to be caused mainly by the fluctuating field produced by paramagnetic impurities through the dipole-dipole interaction. In this system, the relaxation time of the electron between the Zeeman sublevels on the triplet state is longer than the decay time of the triplet state, where electrons on the triplet state are regarded as paramagnetic impurities. If the relaxation time of electrons on the triplet state is negligible, the relaxation time of protons is independent of the laser power. Thus, it is possible to irradiate the laser beam with high power for obtaining the high proton polarization.

However, in the case of molecular crystal, it must be considered that the slow molecular motion as well as the paramagnetic impurities gives rise to the relaxation. In this process, the relaxation time is quite sensitive to the temperature. Thus, it must be taken into account that the heating due to the absorption of laser beam results in shortening of the relaxation time of protons.

Figure 4.9 shows the experimental data on the temperature dependence of the relaxation rate of the proton spin in a pure naphthalene crystal in 940Gauss measured by Schuütz and Wolf[49]. In the temperature region higher than 0°C, the relaxation rate depends strongly on the temperature, it can be explained by the fact that the slow molecular motion in the crystal has the dominant effect on the relaxation.

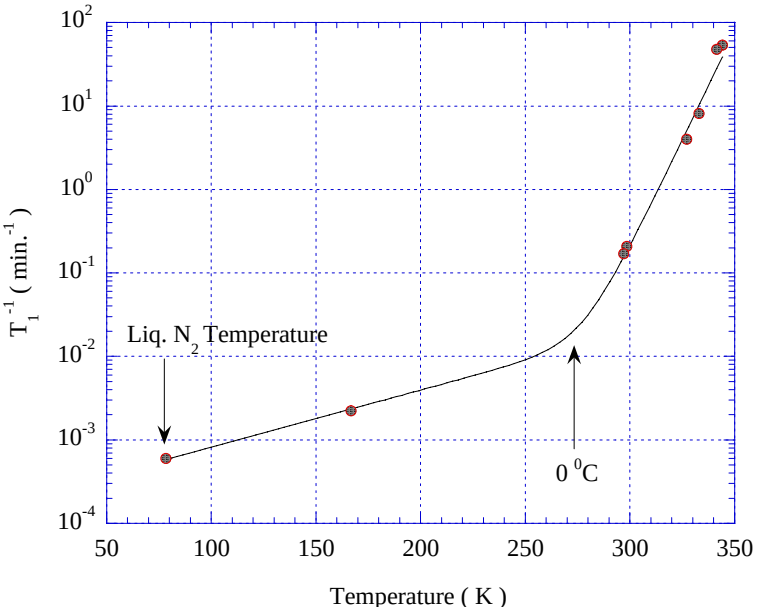

Figure 4.9: Temperature dependence of the relaxation rate of proton in a pure naphthalene crystal[49]. The magnetic field is 940Gauss.

In the temperature region below 250K, the relaxation rate does not depend strongly on the temperature, where the relaxation due to paramagnetic impurities is dominant[49].

In order to investigate the effect of heating to the relaxation rate of protons, first, we measured the relaxation rate of protons in naphthalene doped with 0.01mol% pentacene without irradiation of the laser beam by means of the saturation recovery method at room temperature. The observed relaxation rate was about 1/40minute^{-1}, which was almost the same value as the estimated one from the data obtained by Schuütz and Wolf[49]. In this estimation, it was assumed that the relaxation is caused by the slow molecular motion, where the relaxation rate is proportional to H_0^{-2} when the correlation time of fluctuation is long[49, 51]. This assumption was consistent with our result.

We measured also the relaxation rate during irradiation of CW dye-laser of 40mW as a function of the wavelength of the laser. The results are shown in Figure 4.10. The relaxation rate is the highest at the wavelength of 595nm. If the figure is compared with Figure 3.4, we can find clearly that the relaxation rate is related to the excitation of pentacene. Since decay from the lowest triplet state to the ground state is non-radiative process, the crystal is heated by phonon emission. Therefore, we can conclude that heating of the naphthalene crystal due to the excitation of pentacene by the laser beam gives rise to shorter relaxation time at room temperature.

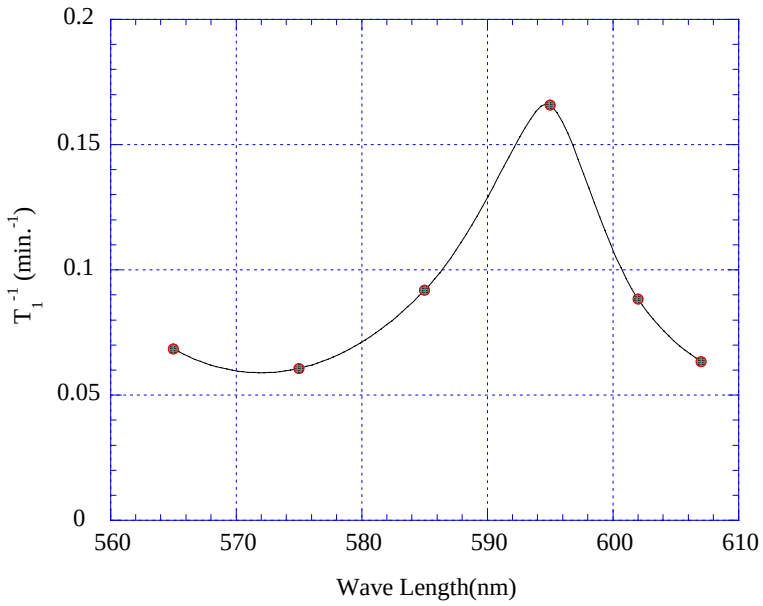

Figure 4.10: The relaxation rate of protons as a function of the wavelength of the CW dye-laser with 40mW at room temperature in 3kGauss. The measurement was performed after polarizing protons by the DNP.

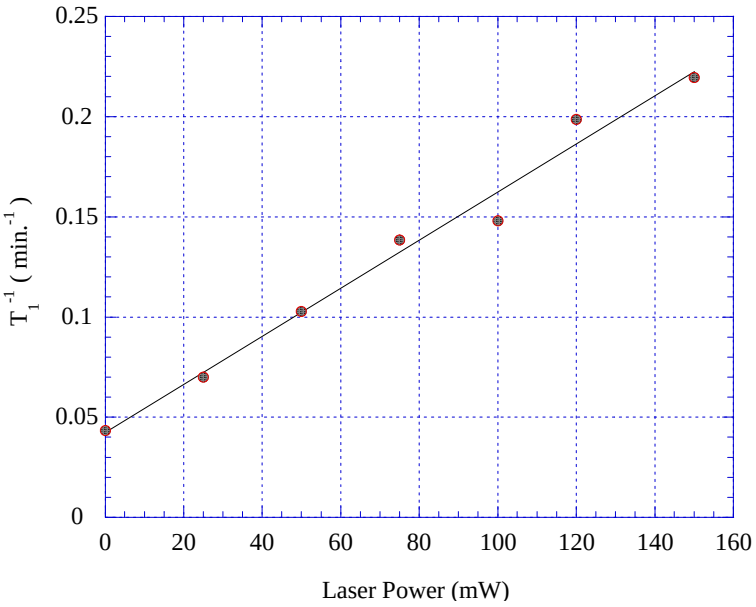

Figure 4.11: The relaxation rate of the proton spin in the crystal of naphthalene doped with pentacene as a function of the laser power in 3kGauss at room temperature during the irradiation of the pulsed dye-laser of 595nm.

Figure 4.11 shows the laser power dependence of the relaxation rate of the proton spin in the crystal of naphthalene doped with pentacene during the irradiation of the pulsed dye-laser. The relaxation rate increases with the laser power. Since the energy of the first singlet state S_1 corresponds to the wavelength of 600nm, pentacene molecules are excited to S_1 directly with the pulsed dye-laser. Then, phonons are emitted in the transition between S_1 and T_0, and the transition between T_0 and the ground state.

The laser power dependence of the relaxation rate during the irradiation of the pulsed N_2-laser with the wavelength of 337nm and the repetition rate of 50Hz is shown in Figure 4.12.

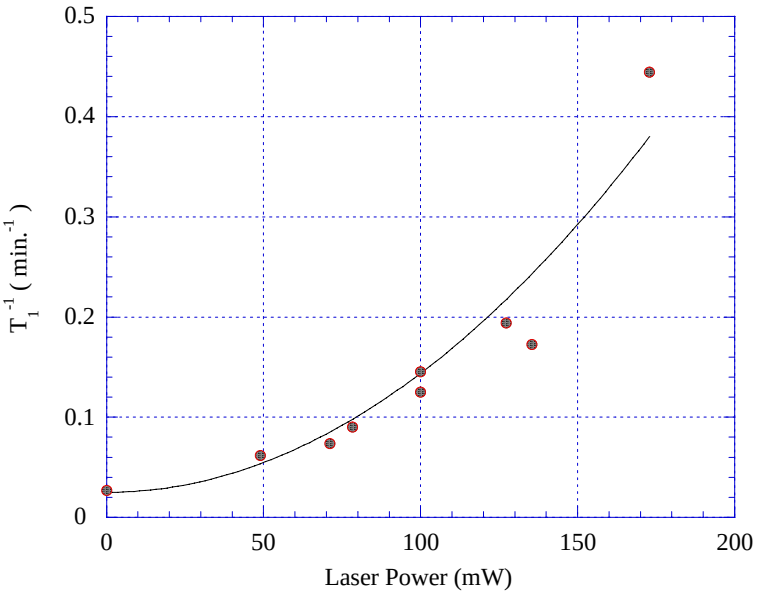

Figure 4.12: The relaxation rate of the proton spin in the crystal of naphthalene doped with pentacene as a function of the laser power in 3kGauss at room temperature during the irradiation of the pulsed N_2-laser of 337nm.

The data are fitted to the square of laser power. This behavior can be explained by the triplet-triplet(t-t absorption) absorption process through the first excited singlet state S_1. It is similar to the two step absorption process. The probability of the t-t absorption of the laser beam of 337nm is higher than that of 595nm[47, 48]. As shown in Figure 4.12, the t-t absorption occurs when the power of the laser beam is higher than 100mW. The phonon emission occurs in the transition between higher excited singlet state and the first excited singlet state S_1 as well as in the transition between higher excited triplet state and T_0. Therefore, the relaxation time of the proton with the N_2-laser has a tendency to be shorter than that with the dye-laser, even though the absorption rate of the N_2-laser beam is lower than that of the dye-laser beam.

Figure 4.13 shows the relaxation rate as a function of the ESR amplitude with the dye-laser and that with the N_2-laser. It was found that the relaxation rate with

the N_2-laser is shorter than that with the dye-laser. The phonon emissions in the transition between a higher singlet state and S_1 as well as the transition between a higher triplet state and T_0 give rise to the large heating effect which leads to shorter relaxation time. Since the t-t absorption is apt to occur by absorption of the light in the ultraviolet region, the ultraviolet light is not preferable as pumping light for pentacene molecule from the viewpoint of the heating effect.

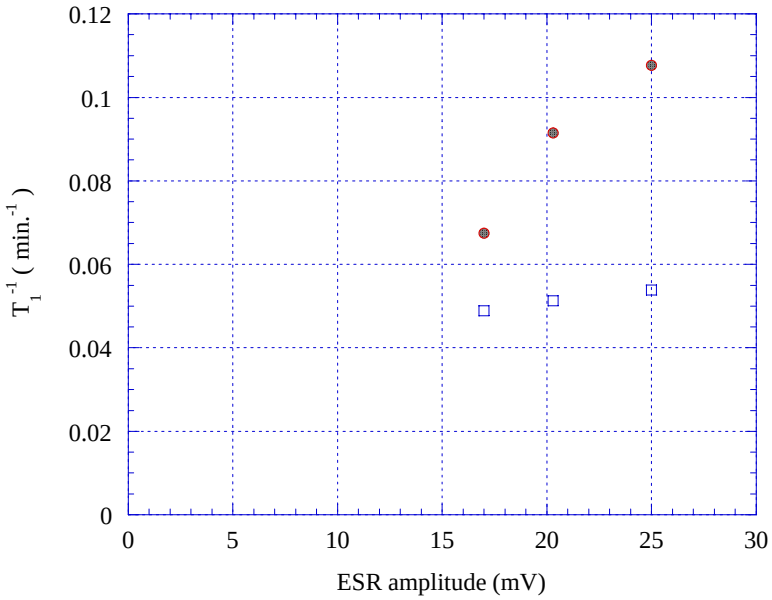

Figure 4.13: The relaxation rate of protons in the single crystal of naphthalene doped with pentacene as a function of the ESR amplitude at room temperature. The solid circles show the results with the pulsed N_2-laser of 337nm and 50Hz. The opened squares show the results with the pulsed dye-laser of 595nm and 50Hz.

In order to minimize the heating effect, the laser power should be optimized to obtain the high proton polarization in the experiment at room temperature.

In the pure naphthalene crystal, there is no significant temperature dependence of the relaxation rate at the temperature lower than 250K as shown in Figure 4.9. In this temperature region, the relaxation due to paramagnetic impurities in the crystal seems to be dominant because it is not the complete crystal. The relaxation time

in the crystal of naphthalene doped with pentacene without irradiation of the laser beam is almost the same as that of the pure naphthalene crystal.

In order to study the contribution of electrons on the triplet state of pentacene to the relaxation time of protons in the low temperature region, we measured the laser power dependence of the relaxation rate of protons in the sample immersed in liquid nitrogen.

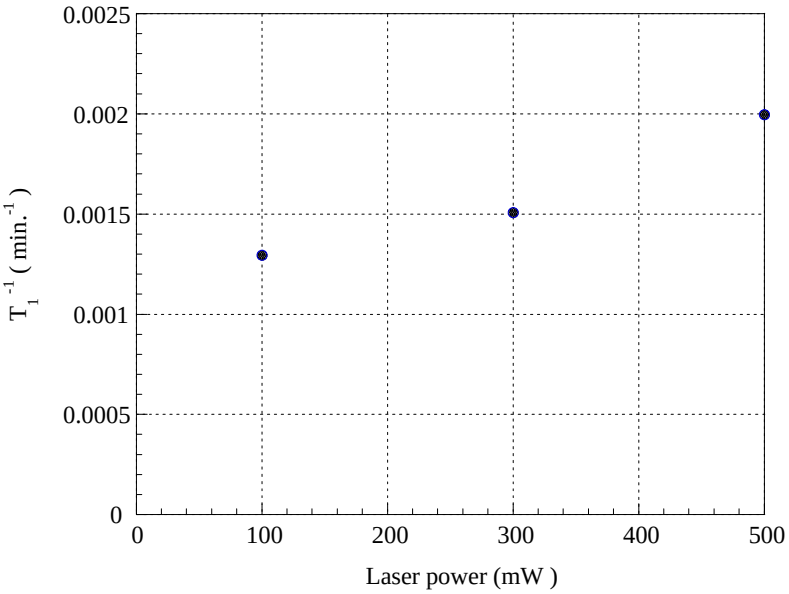

Figure 4.14: The relaxation rate of protons in a naphthalene crystal doped with pentacene as a function of the power of the dye-laser with the wavelength of 600nm and the repetition rate of 50Hz at liquid nitrogen temperature in 3kGauss. The crystal size is 5.5mm×4.0mm×2.3mm.

The result is shown in Figure 4.14. The relaxation rate increases with the laser power. The relaxation rate was 1/500 minutes^{-1} when the power of the dye-laser was 500mW, whereas it was 1/770 minutes^{-1} when the power was 100mW. Such increase of the relaxation rate with power should not be caused only by heating, because the maximum temperature increase of the crystal of 2.3mm in thickness in the liquid nitrogen was calculated to 6.5K with the thermal conductivity of naphthalene of

$0.0118[\mathrm{Wcm^{-1}K^{-1}}]$, even if we assume that all the pentacene molecules are excited and that all the absorbed energy is converted to the heat.

Therefore, we must take into account the fluctuating field produced by the transition from the triplet state to the diamagnetic ground state for understanding the increase of the relaxation rate with power. Such increase of the relaxation rate is interpreted as the increase of the number of electrons on the triplet states. In general, the relaxation rate due to electrons and the spin diffusion of protons is expressed as[1, 2]

$$\frac{1}{T_{1p}} = 4\pi bND, \tag{4.7}$$

where N represents the number of electrons per unit volume and D is the spin diffusion constant. b is called as the "scattering length". Physically it is the distance between an electron and a proton which has equal probability for being flipped by the electron and by a neighboring proton. b is defined as

$$b = 0.7\left(\frac{C}{D}\right)^{\frac{1}{4}}, \tag{4.8}$$

$$C \equiv \frac{2}{5}{\gamma_S}^2{\gamma_I}^2\hbar^2 S(S+1)\cdot\frac{T_{1e}}{1+{\omega_I}^2{T_{1e}}^2} \sim \frac{2}{5}{\gamma_S}^2\hbar^2 S(S+1)\cdot\frac{1}{H_0^2}\cdot\frac{1}{T_{1e}}, \tag{4.9}$$

where γ_S, and γ_I represent the gyromagnetic ratios of the electron and the proton respectively. T_{1e} is the relaxation time of electron, and S is the electron spin. Equation (4.9) is valid, if $\omega_I T_{1e} \gg 1$. In this case, D is the order of $10^{-13}(\mathrm{cm^2/sec})$ [49, 50], and N is the total number of pentacene per unit volume, which corresponds to 0.01mol% if all the pentacene molecules are excited to $\mathrm{T_0}$. From Figure 4.4, T_{1e} is estimated to be the order of 50μsec. If we assume that the lifetime of the triplet state is 20μsec. and that the half of pentacene molecules are excited, the $1/T_{1p}$ is estimated to be 1/3400 $\mathrm{minutes^{-1}}$. If we take into account also the relaxation rate without irradiation of the laser beam, the $1/\mathrm{T}_{1p}$ is estimated to be 1/720 $\mathrm{minutes^{-1}}$. It is

natural to conclude that the change of 'electron polarization' on the triplet state and the relaxation of paramagnetic impurities contribute dominantly to the relaxation process of protons during the irradiation of the laser beam below 250K. Since the contribution of the slow molecular motion is much larger than that of the triplet electrons at room temperature, it is better to perform the DNP at lower temperature than 250K.

P-terphenyl crystal

The temperature dependence of the relaxation rate of protons in the pure p-terphenyl crystal is quite different from that of the pure naphthalene crystal. Figure

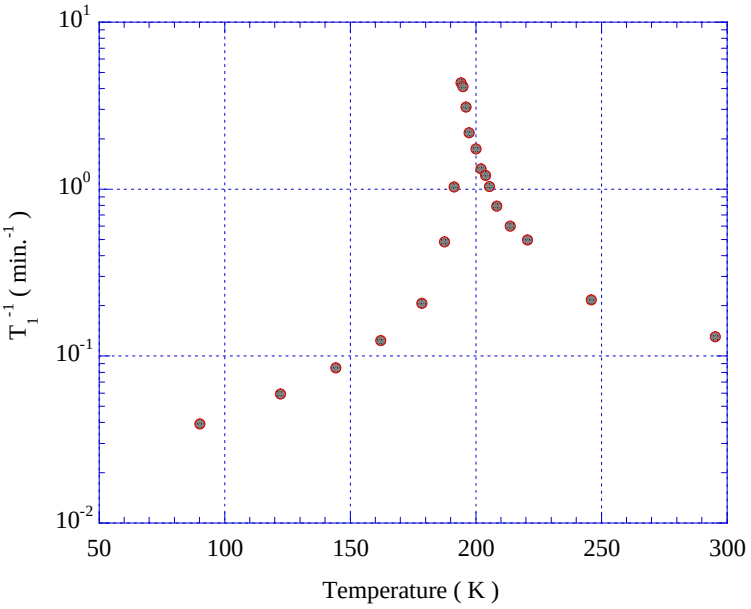

Figure 4.15: Temperature dependence of the relaxation rate of protons in the pure p-terphenyl crystal in 4.64kGauss[46]. The crystal structure is monoclinic($P2_1/a$)/triclinic($P\bar{1}$) at the temperature higher/lower than 193K, respectively.

4.15 shows the temperature dependence of the relaxation rate of protons in a pure p-terphenyl crystal measured by Kouda, et al.[46]. In this crystal, the proton relaxation

rate decreases with the temperature in higher temperature region. Therefore, the laser power seems to have no serious effect on the relaxation rate.

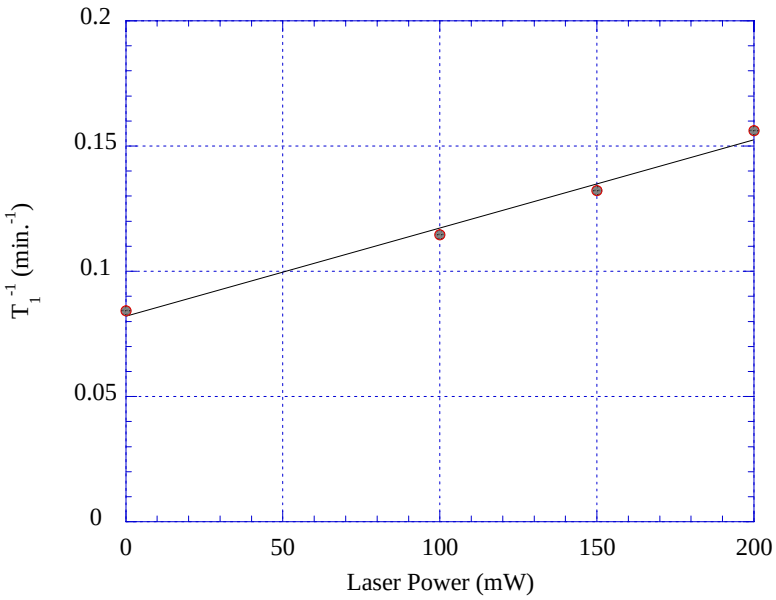

Figure 4.16: Laser power dependence of the relaxation rate of protons in a crystal of p-terphenyl doped with 0.1mol% pentacene in 3kGauss at room temperature with the pulsed dye-laser of 590nm. The measurement of the relaxation rate was performed after polarizing protons by the DNP. The data were fitted to the linear function shown by the solid line.

Figure 4.16 shows the experimental results on the relaxation rate of protons in the p-terphenyl crystal doped with 0.1mol% pentacene as a function of the power of the dye-laser with the wavelength of 590nm and the repetition rate of 50Hz at room temperature.

We measured the relaxation rate of protons in the p-terphenyl crystal doped with pentacene as a function of temperature by two different methods. First, we measured the proton relaxation rate in thermal equilibrium by the saturation recovery method. The results are shown as the open squares in Figure 4.17. Secondly, we measured it after the DNP. The average polarization of protons is about 0.1%. The results are shown as the solid circles in Figure 4.17. Both measurements covered higher temper-

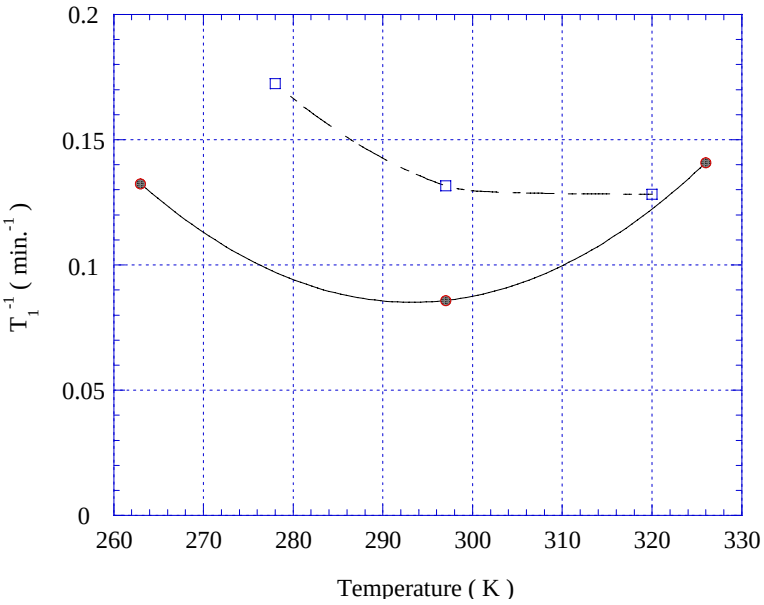

Figure 4.17: Temperature dependence of the relaxation rate of protons in the crystal of p-terphenyl doped with pentacene in 3kGauss. The solid circles show the experimental results for highly polarized protons after the DNP. The polarization of protons is about 0.1%. The open squares show the results in thermal equilibrium without the DNP.

ature region than the measurement in Ref.[46]. The results of the measurement after the DNP shows that the relaxation rate increases with the temperature in higher temperature region. The behavior can be explained if we assume that the relaxation rate of protons in pentacene increases with temperature. This assumption is reasonable because the molecular motion of pentacene and that of naphthalene are similar and the relaxation rate of protons in naphthalene increase with temperature.

On the other hand, the average relaxation rate decreases with the temperature in the temperature region from 200K to 300K. The phenomena can be interpreted by the assumption that the protons in pentacene and those in p-terphenyl participate equally to the relaxation in this energy region, where the relaxation rate of the protons in pentacene is relatively low and the relaxation rate in p-terphenyl decreases with the temperature significantly. This interpretation is consistent with the results of our measurement in the thermal equilibrium and also the results in Ref.[46].

As the result, the relaxation rate has the minimum value at room temperature. Therefore, the laser power must be adjusted to keep the temperature in the optimum value. The p-terphenyl crystal has an advantage for polarizing protons at room temperature, since we can dope pentacene in p-terphenyl with 10times higher concentration than that in naphthalene.

4.4 The results of the proton polarization in naphthalene and p-terphenyl crystal

Naphthalene crystal

As we discussed in the previous sections, we could obtain very high polarization of protons in the single crystal of naphthalene doped with pentacene at the temperature below 250K in 3kGauss. We carried out the DNP of protons in the crystal at liquid nitrogen temperature, since the easiest way to keep the temperature of the crystal lower than 250K is to immerse it in liquid nitrogen.

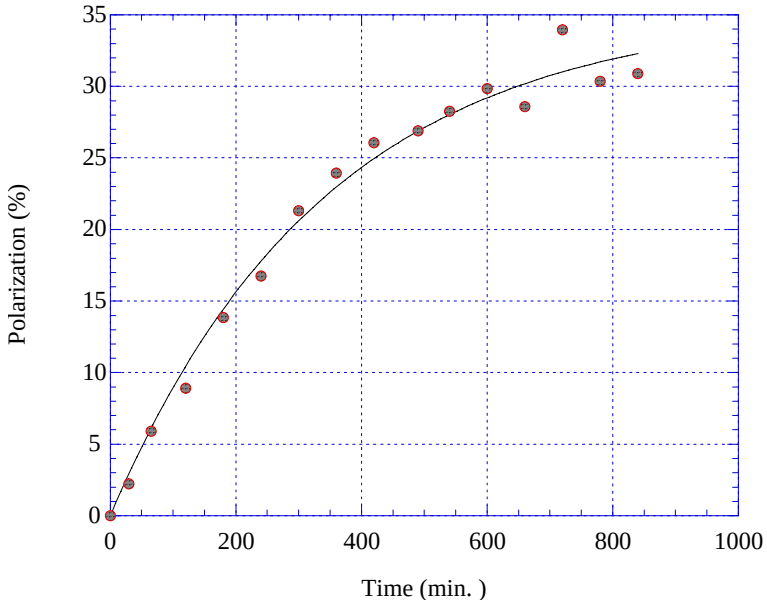

Figure 4.18: Build-up of the proton polarization with the pulsed dye-laser of 600nm, 350mW, 50Hz as a function of time in 3kGauss at liquid nitrogen temperature. A single crystal of naphthalene doped with about 0.001mol% pentacene was used. The build-up time of 343 minutes and the extrapolated maximum proton polarization P_0^{exp} of 35.3% were obtained by fitting the data to Equation (2.19).

Figure 4.18 shows the result on the build-up of the polarization, where the pulsed dye-laser with the wavelength of 600nm and the average power of 350mW was ap-

plied. The repetition rate was 50Hz. The crystal was naphthalene doped with about 0.001mol% pentacene. The wavelength of the absorption peak was 600nm at liquid nitrogen temperature, while it was 595nm at room temperature. The sweep width of the field was 42Gauss, and the sweep duration was 10μsec. The polarization of 30% was obtained after the irradiation of the laser beam and microwaves for 12 hours. The build-up time is long since the pentacene concentration in this crystal is very low. When we use a crystal doped with 0.01mol% pentacene, the build-up time is about one hour with the dye-laser of higher power. The result can be compared to that with the N_2-laser[52]. The obtained polarization is substantially higher than the

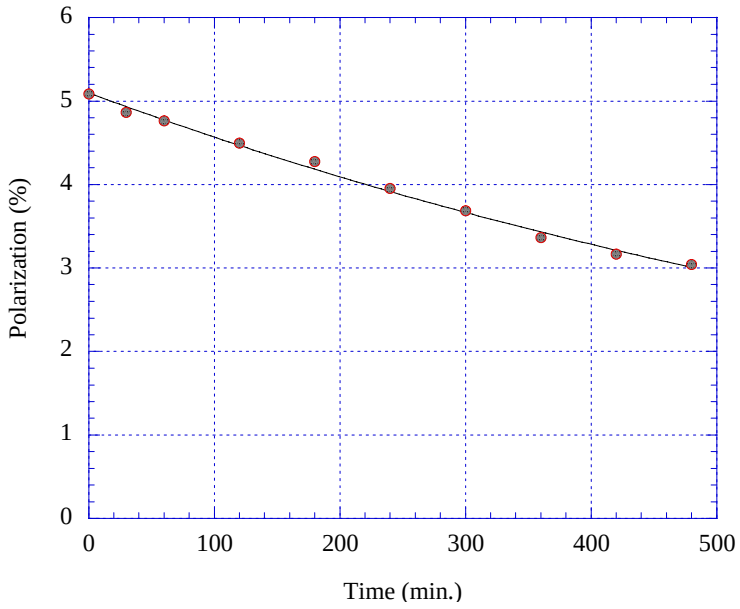

Figure 4.19: Decay curve of the proton polarization in 3kGauss at liquid nitrogen temperature in irradiation with the pulsed dye-laser of 600nm, 250mW, and 50Hz. The relaxation time is 909 minutes.

value reported by Henstra, et al.[33]. This is partly because the relaxation time at liquid nitrogen temperature is much longer than that at room temperature. It was also quite helpful that the crystal was irradiated with the high power laser beam without serious shortening of the relaxation time of protons at liquid nitrogen temperature.

Figure 4.19 shows the decay curve of the proton polarization during irradiation of the dye-laser of 250mW and 50Hz. The number of excited pentacene molecules was saturated with the laser power. By fitting Figure 4.18 to the Equation(2.19), we obtained the build-up time T_{build} and the extrapolated maximum proton polarization P_0^{exp}, that is $T_{build} = (\bar{A}+\Gamma)^{-1} = 343$ minutes and $P_{p0}^{exp} = 35.1\%$. The relaxation time was obtained as $T_{1p} = \Gamma^{-1} = 909$ minutes from Figure 4.19. The ESR amplitude was measured to obtain the average of 'electron polarization' $\bar{P}_e$ before the DNP. We found that $\bar{P}_e$ was 62.5%. Assuming that Equation (2.22) is applicable to this measurement, P_{p0} was calculated by using the values of $\bar{A}$, Γ, and $\bar{P}_e$ as

$$P_{p0} = \frac{\bar{A}}{\bar{A}+\Gamma} \cdot \bar{P}_e = 38.9\%. \tag{4.10}$$

It is consistent with the experimental extrapolated value P_{p0}^{exp}. For obtaining higher polarization, it is important to find out more suitable crystal for the DNP. We will be able to obtain the same amount of proton polarization at higher temperature than liquid nitrogen temperature.

We tried to obtain high proton polarization at a temperature higher than 250K. For this purpose the optimization of the laser power was necessary. We used the crystal whose relaxation time was 19.5 minutes without laser beam at room temperature in 3kGauss. The relaxation time was 8.0 minutes in the presence of the pulsed dye-laser with the wavelength of 595nm, the average power of 100mW, and the repetition rate of 50Hz. The conditions for the polarization transfer were the same as in the experiment at liquid nitrogen temperature. The proton polarization of 0.12% was obtained after 40 minutes irradiation of the laser beam and the microwaves. It corresponds to the enhancement of 1200. In order to obtain higher polarization at room temperature, it is considered to use other host crystals which have different temperature dependence of the proton relaxation time.

P-terphenyl crystal

The DNP of protons in p-terphenyl requires similar optimization procedure as in the case of naphthalene crystal. We used the crystal doped with 0.1mol% pentacene. The relaxation time of protons was 11.9 minutes without the laser beam at room temperature and 7.6 minutes during the irradiation of the pulsed dye-laser of the wavelength of 590nm, the power of 150mW and the repetition rate of 50Hz. The polarization of 1.3% was obtained at room temperature, while the polarizing time was 60 minutes. This polarization corresponds to the enhancement of 13,000. It is 10 times as high as the one in naphthalene crystal. It is ascribed to higher pentacene density in p-terphenyl crystal.

In order to obtain higher polarization, the optimization of parameters and finding the best crystal is important as in the case of naphthalene crystal. $1/T_{1p}$ in pure crystal is about 1/30 minutes^{-1} at liquid nitrogen temperature as shown in Figure 4.15. On the other hand, $1/T_{1p}$ is calculated to be 1/100 minutes^{-1} from Equation (4.7), (4.8) and (4.9) assuming that all of pentacene are excited. Thus it is expected that the relaxation rate is not so large compared to $1/T_{1p}$ in pure crystal. Therefore, it is possible to obtain the high polarization with the high power laser beam at liquid nitrogen temperature. The obtained polarization in the crystal of p-terphenyl doped with 0.1mol% was about 19% after 120 minutes irradiation of the pulsed dye-laser with the wavelength of 590nm, the power of 500mW and the repetition rate of 50Hz in 3kGauss at liquid nitrogen temperature. Higher polarization will be obtained if we prepare better crystal.

Chapter 5

Application to the polarized target

5.1 Measurement of proton polarization by neutron transmission

The proton polarizations in the naphthalene crystal and p-terphenyl crystal were measured by the slow neutron transmission through the crystal. The values were compared to the ones obtained by the NMR measurement.

In low energy neutron-proton scattering, the scattering cross section for the neutron whose spin is parallel to the proton spin σ_{para} is 20 times as large as the one whose spin is anti-parallel to the proton spin $\sigma_{antipara}$. We define the polarization cross section σ_p as $\sigma_p = 1/2 \cdot (\sigma_{antipara} - \sigma_{para})$. The large polarization cross section for n-p scattering in the wide energy range allows us to use the polarized proton filter as a polarizer of the neutron beam[23, 24, 25]. The detailed discussion of the neutron polarizer is described in Section 5.2.

The total cross sections $\sigma_{\pm}$ of the neutrons with spin up and spin down to the direction of the proton polarization P_p of the target can be expressed as[18, 23]

$$\sigma_{\pm} = \sigma_0 - \sigma_1 P_p^2 \mp \sigma_p P_p, \tag{5.1}$$

where, σ_0 is the cross section averaged over the directions of the neutron spin and proton spin, $\sigma_1 P_p^2$ corresponds to the term proportional to the square of the proton polarization P_p. This term is independent of the neutron spin. The transmission T_{pol} of the unpolarized neutron beam through the polarized proton filter of thickness t, the number density of protons n, and the proton polarization P_p is described as

$$T_{pol} = T_{unpol} \cdot \exp(P_p^2 n \sigma_1 t) \cdot \cosh(P_p n \sigma_p t), \tag{5.2}$$

where, T_{unpol} is the transmittance of the unpolarized neutron through the unpolarized proton filter. It is expressed as

$$T_{unpol} = \exp(-n\sigma_0 t). \tag{5.3}$$

In order to know the proton polarization in the filter material, we measured $\gamma_1 \equiv T_{pol}/T_{unpol}$. The proton polarization can be derived from the equation

$$P_p = \left(\frac{\gamma_1 - 1}{1/2 \left(\sigma_p/\sigma_0\right)^2 \left(ln\gamma_2\right)^2 - \sigma_1/\sigma_0 \left(ln\gamma_2\right)} \right)^{\frac{1}{2}}, \tag{5.4}$$

where $\gamma_2 \equiv T_{unpol}/T_{empty}$. T_{empty} is the transmission of the unpolarized neutron through the equipment without proton. Since $P_p \sigma_p nt \ll 1$ and ${P_p}^2 \sigma_1 nt \ll 1$, the 3rd order terms of P_p in Equation (5.2) were neglected. For neutrons of about 1meV, the ratios of σ_p to σ_0, and that of σ_1 to σ_0 are independent of material[23]. $\sigma_p/\sigma_0 \sim 2/3$, and $\sigma_1/\sigma_0 \sim 1/3$ were taken for obtaining the target polarization.

We carried out the experiment of the neutron transmission using the neutron in the cold neutron beam line SAN at KEK-KENS. The experimental setup is shown in Figure 5.1. The energy of the neutron was 1meV∼3meV and the beam intensity was $2\times10^4/\mathrm{cm}^2/\mathrm{sec}$. The beam was collimated to be 0.6cm×0.3cm at the filter with two collimators made of cadmium. Crystals of naphthalene and p-terphenyl doped with pentacene of 0.01mol% and 0.1mol% respectively, were used as filter materials. The crystals were 0.8cm high, 0.5cm wide and 0.3 in thickness. They were put in a quartz-glass dewar which was filled with liquid nitrogen.

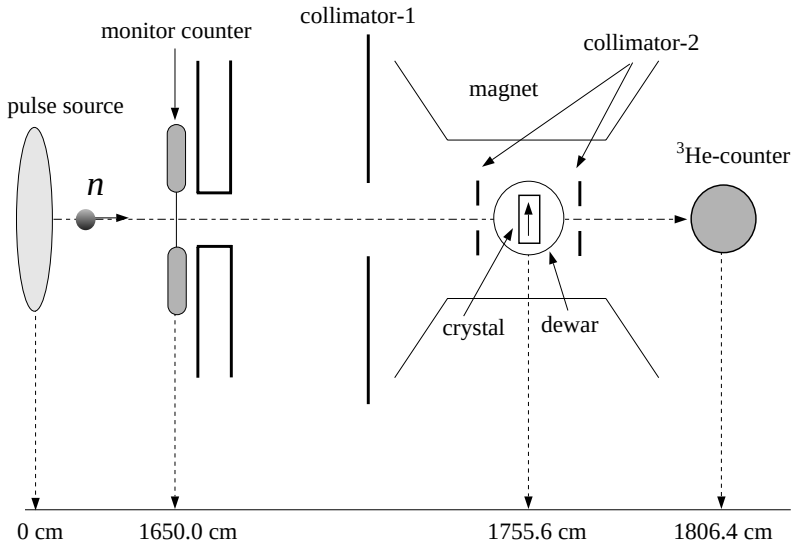

Figure 5.1: The top view of the setup of neutron transmission measurement. The energy of pulse neutron beam is 1meV to 3meV. The unpolarized neutron beam was collimated to be 0.6cm(hight) × 0.3cm(width) at the filter with two collimators made of Cd. The crystal size was 0.8cm(hight) × 0.5cm(width) and the thickness was 0.3cm. The magnetic field was set to be 3kGauss and 7Gauss.

First, the proton in the naphthalene crystal immersed in liquid nitrogen was polarized by the DNP using the pulsed dye-laser of 500mW. After irradiation of the laser beam and microwaves for about two hours, we measured the neutron transmission. In order to obtain the proton polarization in naphthalene using Equation (5.4), we had to know the transmission of the unpolarized neutron through the unpolarized filter T_{unpol}. It was obtained by means of the extrapolation of the decay curve of "the

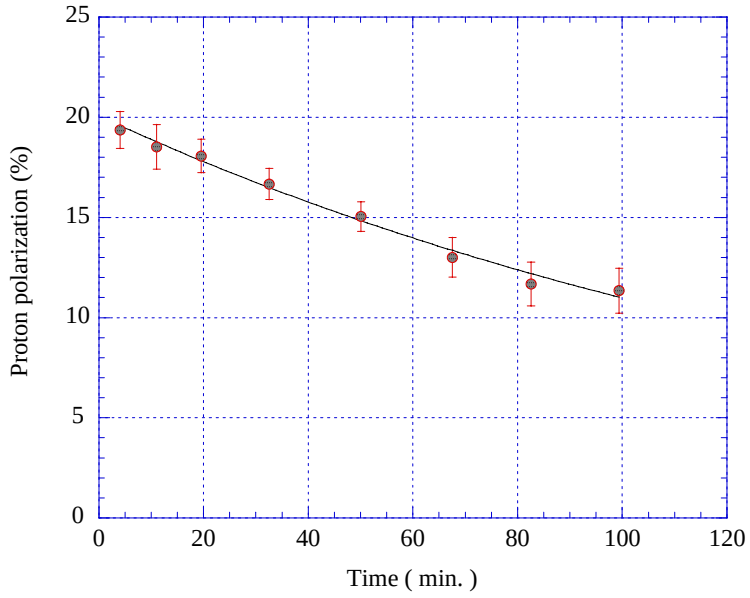

Figure 5.2: Decay of the proton polarization in a naphthalene filter without laser beam in 7Gauss at liquid nitrogen temperature measured by the neutron transmission method. The proton polarization and T_{1p} were obtained to be 20.0%±3.6% and 166 ± 22 minutes respectively.

transmission of neutrons through the polarized proton filter" to "the transmission of neutrons through the unpolarized filter", since it was difficult to prepare an unpolarized filter. The proton polarization obtained from the neutron transmission was 20.0±3.6%, which was consistent with the value measured by the NMR mentioned in Chapter 4.

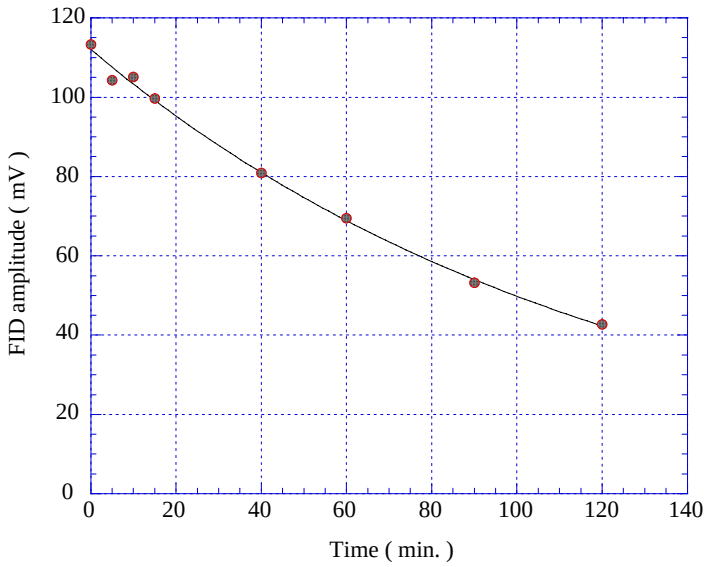

Figure 5.3: Decay of the proton polarization in a naphthalene crystal in 5Gauss at liquid nitrogen temperature by means of the NMR method. T_{1p} was obtained to be 123 minutes.

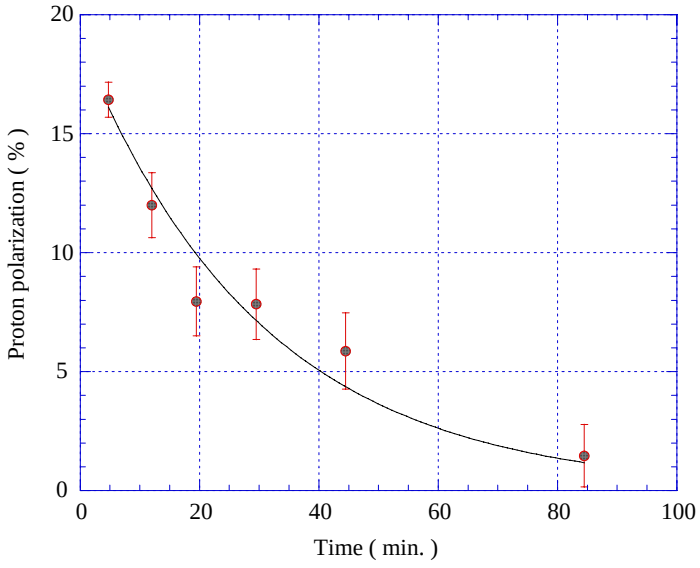

Figure 5.4: The proton polarization in p-terphenyl in 3kGauss at liquid nitrogen temperature as a function of time measured by the neutron transmission method. The solid line shows the curve fitted to an exponential function. The proton polarization and the relaxation time were 18.9±1.2% and 30.0 ± 5.5 minutes respectively.

The measurement of the relaxation time of proton by the neutron transmission method was made in the field of 7Gauss without irradiation of the laser beam and microwaves. The proton polarization as a function of time is shown in Figure 5.2. The obtained relaxation time of proton was 166 ± 22 minutes. The relaxation time measured by the NMR in 5Gauss was 123 minutes as shown in Figure 5.3. These values are consistent with each other, if we take account of the difference of the magnetic fields. The relaxation time is surprisingly long even in such a low magnetic field.

The decay of the proton polarization in p-terphenyl in 3kGauss at liquid nitrogen temperature is shown in Figure 5.4. The initial polarization was $18.9 \pm 1.2\%$. The relaxation time was obtained to be 30.0 ± 5.5 minutes. The relaxation time measured by the NMR method under the same condition was 33 minutes. Both values are consistent with each other.

5.2 Polarized proton filter for obtaining a polarized slow neutron beam

As we discussed in Section 5.1, the polarized filter can be used for polarizing neutron beams. An unpolarized neutron beam becomes polarized after it passes through a polarized proton filter as shown schematically in Figure 5.5. From Equation

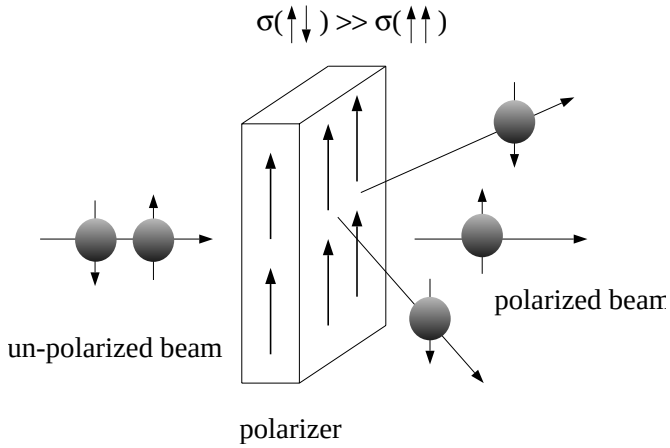

Figure 5.5: Spin filter for polarizing neutron beam

(5.1), the polarization P_n and the transmission T_n of the neutron after passing through the polarized filter are described as

$$P_n \cong \tanh(P_p n \sigma_p t), \tag{5.5}$$

$$T_n \cong T_0 \cosh(P_p n \sigma_p t). \tag{5.6}$$

These equations are valid, if the energy of the neutron is higher than 0.3eV, where σ_1 can be neglected for the neutron with energy higher than 0.3eV[18, 23]. If we use thicker crystal, the polarization of the neutron is higher and the transmission is lower. For optimization of the thickness of the crystal, the figure of merit(FOM) is defined as the product of the polarization and the square of the transmission of the neutron[18]. The figure of merit has the largest value, when the thickness of the crystal is 1.5cm

and the neutron energy is 1eV, if the polarization of the protons is 60%.

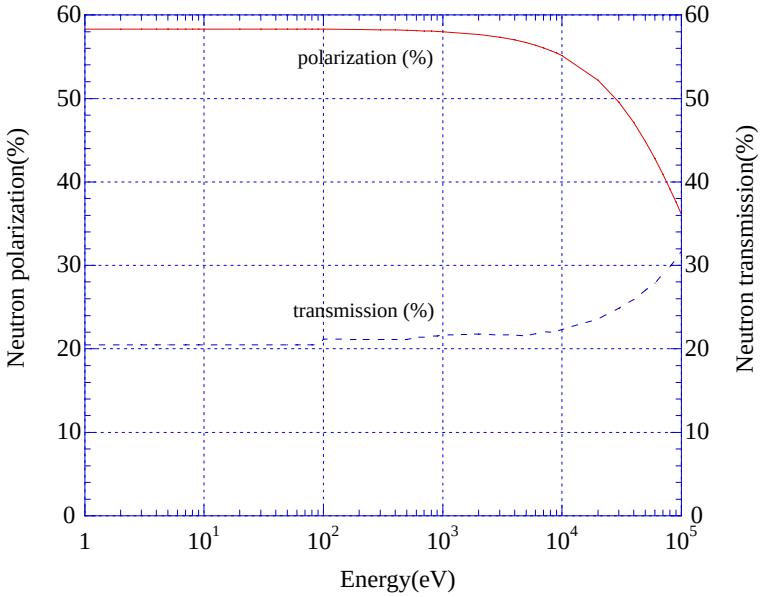

Figure 5.6: The polarization(solid line) and transmission(broken line) of the neutron beam after passing through the naphthalene crystal whose thickness is 1.5cm, when the neutron energy is 1eV. The polarization of the proton in the crystal is assumed to be 60%.

The polarization cross section σ_p depends on the neutron energy as

$$\sigma_p = \frac{16.7(1 + E_n/6300)}{(1 + E_n/133)(1 + E_n/4150)} \text{ (barn)}, \tag{5.7}$$

in the energy region of 1eV $\leq E_n <$ 1MeV, where E_n is the neutron energy in the unit of keV.

Figure 5.6 shows the energy dependence of the polarization and transmission of the neutron calculated by Equation(5.5), (5.6) for naphthalene crystal, where the proton polarization is 60% and the crystal thickness is 1.5cm. The neutron polarization of 59% and the transmission of about 20% can be obtained for neutrons in the energy region from 1eV to 10^4eV. The characteristics on neutron polarization and transmission in the case of p-terphenyl crystal are almost the same as those in the case of naphthalene crystal.

5.3 Polarized proton target

If we compare the hydrogen density and the ratio of the number of the free protons to that of the protons bound in nuclei(dilution factor) in target materials, naphthalene and p-terphenyl are not advantageous over other materials(Table 5.1). However, these materials have advantages over other materials for experiments in which high beam intensity or low momentum particles are used.

Target material	Dilution factor	Hydrogen density (g/cm^3)	Temperature (K)	Magnetic field (kGauss)	Ref.
Propanediol	0.190	0.11	0.5	25	[11]
Butanol	0.238	0.11	0.5	25	[8, 9]
Ethylene glycol	0.176	0.11	0.5	25	[5, 6]
Ammonia	0.300	0.14	0.5	25	[13]
			1.0	50	[14]
Naphthalene	0.118	0.072	77	$\sim$3	
P-terphenyl	0.115	0.076	77	$\sim$3	

Table 5.1: Comparison of naphthalene and p-terphenyl to other target materials. The dilution factor is the ratio of the number of the free protons to that of the protons bound in nuclei.

Here, we consider the naphthalene crystal, since the relaxation time of protons in naphthalene crystal is longer than that in p-terphenyl at the temperature below 250K.

Heating and the radiation damage due to the beam causes the depolarization in the ordinary polarized target operated at the temperature lower than 1K in the high intensity beam. Heating with the beam of charged particles shortens the relaxation time of the protons. In addition, free electrons which causes the relaxation of protons are produced by irradiation of the charged particles. It is noticed that the recombination of ions produced by radiation damage does not occur at the temperature lower

than 1K.

In order to suppress heating with the beam, the target is usually composed of many small beads, the sizes of which are about 0.1cm in diameter. The beads are immersed in the bath of the refrigerator in order to keep the good heat contact between the material and the bath. Even if such beads are used for the target material, the temperature increase by heating with beam is serious in the case of the spin frozen target. Therefore, the beam intensity is limited to be less than $10^7 \sim 10^8$/cm^2/sec.

The relaxation time of proton in pure naphthalene is insensitive to the temperature lower than 250K as shown in Figure 4.9. Consider a cylindrical naphthalene sample of 2cm in diameter, 1cm in thickness, whose thermal conductivity is 0.0118 W/cm^2/sec. If the electron beam, whose intensity is 1.7×10^{11}/cm^2/sec. is irradiated on the crystal immersed in liquid nitrogen, the temperature increase is about 0.1K which does not affect the relaxation time. If we put the electron beam whose intensity is 5.0×10^{12}/cm^2/sec., the temperature increase at the center of the crystal is about 30K which gives rise to the increase of the relaxation rate by factor 1.5 according to our estimation. It was calculated using the data in 940Gauss[49] with the assumption that the relaxation rate is proportional to $H_0^{-1/2}$ in this temperature region as shown in Equation (4.7), (4.8) and (4.9). When the target is composed of thin pieces of 0.1cm in thickness, the temperature increase is 0.3K. From these considerations, it is expected that the depolarization due to the beam heating is negligible for very high intensity beam.

The polarization of proton decreases due to the radiation damage if the temperature of the target material is very low. The depolarization obeys the formula[53]

$$\frac{P_p}{P_{p0}} = e^{-\varphi/\varphi_0}, \tag{5.8}$$

where P_{p0} is the initial polarization before irradiation, φ is the radiation dose. The

characteristic dose φ_0 is 3.7×10^{14} electrons/cm^2 in butanol[53]. The characteristic dose of ammonia is 30 times as high as that of butanol[54]. It is necessary to warm up the target material for recovery of the proton polarization. When the temperature of butanol rises to about 120K, the recombination of ions occurs[53]. The ammonia target needs to warm up to 80K[55]. The recombination of ions in naphthalene occurs at liquid nitrogen temperature. Thus, it is expected that the naphthalene target is much stronger than other target material for radiation damage.

The polarized proton target of naphthalene crystal has another advantage over the ordinary cryogenic targets. Since the proton is polarized at a temperature higher than that of liquid nitrogen, the target can be used for scattering experiments in the vacuum chamber without wall for the crystal, if it has a good thermal contact with liquid nitrogen or other cold material. Such a polarized proton target is useful for scattering experiments with low momentum particles, because there is no material other than naphthalene in the path of the beam.

The proton is polarized in the field of 3kGauss and it has a quite long relaxation time even in the field of 5Gauss. Therefore, there are practically no field effect on the trajectories of the incident and scattered particles, even if the energies of the particles are very low.

Chapter 6

Conclusion

We have carried out the experiment to polarize protons in single crystals of naphthalene and p-terphenyl doped with pentacene using a dye-laser. The experiment was performed in the magnetic field of 3kGauss at room temperature and liquid nitrogen temperature. Protons have been dynamically polarized by transferring the difference of the populations between two Zeeman sublevels of the photoexcited triplet state of pentacene molecule to the proton polarization by means of the integrated solid effect.

In order to polarize protons in the crystal dynamically, first, pentacene molecules were excited to the lowest triplet state through singlet excited states by means of laser excitation. Just after applying a pulsed laser beam to the crystal, the microwave was irradiated during the lifetime of the triplet state(about 20μsec.) and simultaneously the external field was swept. The proton polarization increased by repeating this cycle. The population differences between the Zeeman sublevels of the triplet state was calculated by the analysis of the time evolution of the ESR amplitude. It has been confirmed that the 'electron polarization' between the two Zeeman sublevels $|0>$ and $|-1>$ is about 70%. By the measurement of the external field dependence of the proton polarization, we have confirmed that the DNP due to the integrated solid effect has worked efficiently.

We measured the relaxation rate of the proton in a pentacene-doped naphthalene crystal during irradiation of the laser beam. It was found that the relaxation rate of protons in the naphthalene crystal increases with laser power significantly at room temperature. The result could be explained by the fact that the relaxation is mainly attributed to the slow molecular motion.

On the other hand, the relaxation rate was found to be low but increases slightly with laser power if the crystal was immersed in liquid nitrogen. To understand the phenomena, we must take into account the fluctuating field produced by the decrease of the 'electron polarization' on the triplet states of the pentacene molecule as well as the relaxation due to paramagnetic impurities in the crystal, whereas the contribution of the slow molecular motion is negligibly small.

We found that the laser power dependence of the relaxation rate during irradiation of the N_2-laser(λ=337nm) is more significant than that with the dye-laser(λ=595nm). The result was interpreted as the photon absorption in the transition between higher excited triplet state and the lowest triplet state which is apt to occur with ultra-violet light.

From these results we concluded that it is preferable to irradiate the pulsed dye-laser on the crystal immersed in liquid nitrogen for our purpose. We obtained 30% polarization of protons in naphthalene doped with pentacene (0.001mol%) using the pulsed dye-laser with the wavelength of 600nm, the average power of 350mW and the repetition rate of 50Hz in 3kGauss at liquid nitrogen temperature. The maximum polarization at room temperature was 0.12% by using the dye-laser of 595nm, 100mW and 50Hz.

We could dope pentacene molecules in p-terphenyl with higher concentration (0.1mol%) than in naphthalene. Although the laser power dependence of the pro-

ton relaxation in this crystal is not so significant as that in naphthalene crystal at room temperature, the laser power must be optimized for obtaining the high polarization. We obtained the proton polarization of 1.3% at room temperature with the pulsed dye-laser of 590nm, 150mW and 50Hz. The polarization of 19% was obtained with the dye-laser of 590nm, 500mW and 50Hz at liquid nitrogen temperature.

The proton polarization obtained by the DNP at liquid nitrogen temperature was also measured by the neutron transmission method using neutrons with the energy of 1meV to 3meV. The idea comes from the fact that in low energy neutron-proton scattering the cross section for the neutron with spin parallel to the proton spin is much larger than that with anti-parallel spin. We confirmed that the polarization measured by the neutron transmission method is consistent with that measured by the NMR method.

It was also found that the relaxation time of protons in 7 Gauss at liquid nitrogen temperature is about 160 minutes, which is surprisingly long compared to that in other organic crystals.

The method mentioned in this dissertation have the advantages on the resistance for the radiation damage and beam heating over the ordinary polarized proton targets. Furthermore, it is useful for scattering experiments with low momentum particles.

Acknowledgments

I would like to take this opportunity to thank many people who have helped me during my time in graduated school.

First of all, I would like to express my sincere gratitude to my supervisor, Professor Akira Masaike. Under his guidance, I have had opportunity to join experiments on the dynamic nuclear polarization and fundamental physics with neutrons. His continuous support, advice and encouragement have helped me to keep my interests and motivation. I greatly appreciate his comments and careful review of my dissertation.

I am grateful to Professor Tsutomu Yabuzaki who is the group reader of the quantum optics group. The experiment of the dynamic nuclear polarization was carried out with the experimental facilities of his group. I sincerely thank him for the supports and encouragement.

I would like to appreciate Professor Yoshiro Takahashi and Professor Hirohiko Shimizu who introduced the present work to me. The advice, discussion and the instruction on the solid state physics of Professor Takahashi, has helped me to execute the present experiment on the DNP. I thank him also for valuable comments on the manuscript. I appreciate Professor Hirohiko Shimizu for the instruction, discussion and encouragement on the polarized proton filter and neutron physics. The experiment with the neutron beam would not have been possible without him.

I really want to express my special thanks to Professor Hideto En'yo. His advice,

support and powerful encouragement are appreciated very much. I am also grateful to Professor Kenichi Imai for his comments and advice. He encouraged me to realize the polarized proton target.

The execution of the present experiment has been supported by many individuals. Mr. Ryoji Takizawa constructed the equipments and established the technique for the crystal growth. The tireless efforts of Mr. Ippei Shaké helped me strongly. Mr. Masahiro Oda gave me several unique ideas for pursuing the present experiment. I am indebted to them for their assistance, encouragement and friendship. I am thankful to Professor Noboru Hirota and Professor Motohide Terazima for the useful discussion and helpful comments on the crystal growth, the photoexcited triplet state and the ESR detection. Thanks are also due to Emeritus Professor Tsuneo Hashi, Professor Motomasa Daigo, Professor Kenichi Kanno for comments, advice and guidance. I also express my thanks to Professor J. Schmidt in University of Leiden for the useful advice on the present experiment for the DNP.

The work on the experiment with the neutron beam was supported by the following people. I owe to my acknowledgment to Professor Michihiro Furusaka who is responsible for the cold beam line BSF-SAN at KEK. I want to show my sincere gratitude to Mr. Takayuki Oku and Mr. Yukio Ogawa for assistance and friendship for the experiment in BSF-SAN. I am grateful to Professor Kimio Morimoto, Professor Shigeru Ishimoto and Professor Yasuhiro Masuda of KEK for useful comments and advice on the DNP, NMR and the polarized proton filter.

I also would like to express my appreciation to Professor Koichiro Ashahi, Dr. Kenji Sakai and Dr. Hiromi Sato of Tokyo Institute of Technology. Much discussion on the polarized spin filter and the fundamental physics with neutrons, and the encouragement have helped me to maintain my interest.

I wish to thank all the members of the group for particle and nuclear physics (PN-group) and the group for quantum optics for their advice, discussion and friendship. In particular, I want to show my gratitude to Mr. Yasuyuki Matsuda and Mr. Kenichi Okumura. We have enjoyed discussion on fundamental physics, and have strongly affected to each other. I also thank Dr. Akihiro Fujisaki and Dr. Toshiya Kinoshita for discussion on solid state physics, atomic physics and optical physics. It was a pleasure to discuss the subjects on various fields of physics with them.

I am grateful to Ms. Michiyo Masaike for her heartfelt support and hospitality. I also thank Ms. Mari Hayashi for secretarial works and her kindness in PN group. I wish to appreciate Ms. Keiko Nakagawa and Ms. Eiko Takahashi for their clerical works, encouragement and hospitality.

This work has been partially supported by Fellowships of the Japan Society for the Promotion of Science for Japanese Junior Scientists.

Finally I express my great thanks to my parents, Kenichi and Shigeko Iinuma and my sister, Yukari Ohashi for their continuous support and patience during my time in graduate study.

Bibliography

[1] C. D. Jeffries, *Dynamic Nuclear Orientation*, (Interscience Publishers, New York, 1963).

[2] A. Abragam, *The Principles of Nuclear Magnetism*, (Clarendon Press, Oxford, 1961).

[3] A. Abragam, and M. Goldman, *Nuclear Magnetism : Order and Disorder*, (Clarendon Press, Oxford, 1982).

[4] M. Borghini, Proceedings of 2nd International Conference on Polarized Targets, Berkeley, 1971, (National Technical Information Service, Virginia, 22151, U.S.A.) p.1.

[5] A. Masaike, H. Glattli, J. Ezratty, and A. Malinovski, *Phys. Lett.* **30A**, (1969) 63.

[6] M. Odehnal, and V. Bouffard, *Phys. Lett.* **32A**, (1970) 407.

[7] H. Glättli, Proceedings of 2nd International Conference on Polarized Targets, Berkeley, 1971, (National Technical Information Service, Virginia, 22151, U.S.A.) p.281.

[8] D. A. Hill, J. B. Ketterson, R. C. Miller, A. Moretti, R. C. Niemann, L. R. Windmiller, and A. Yokosawa, *Phys. Rev. Lett.* **23**, (1969) 460.

[9] S. Mango, Ö. Runólfsson, and M. Borghini, *Nucl. Inst. Meth.* **72**, (1969) 45.

[10] G. Hartmann, D. Hubert, S. Mango, C. C. Morehouse, K. Plog, Proceedings of 2nd International Conference on Polarized Targets, Berkeley, 1971, (National Technical Information Service, Virginia, 22151, U.S.A.) p.289.

[11] W. de Boer, *Nucl. Inst. Meth.* **107**, (1972) 99.

[12] K. Scheffler, Proceedings of 2nd International Conference on Polarized Targets, Berkeley, 1971, (National Technical Information Service, Virginia, 22151, U.S.A.) p.271.

[13] T. O. Niinikoski, and J.-M. Rieubland, *Phys. Lett.* **72A**, (1979) 141.

[14] D. G. Crabb, C. B. Higley, A. D. Krisch, R. S. Raymond, T. Roser, J. A. Stewart, and G. R. Court *Phys. Rev. Lett.* **64**, (1990) 2627.

[15] S. Isagawa, S. Ishimoto, A. Masaike, and K. Morimoto, *Nucl. Inst. Meth.* **154**, (1978) 213.

[16] S. Ishimoto, S. Isagawa, A. Masaike, and K. Morimoto *Nucl. Inst. Meth.* **171**, (1980) 269.

[17] S. Ishimoto, S. Hiramatsu, S. Isagawa, K. Morimoto, and A. Masaike, *Jpn. J. Appl. Phys.* **28**, (1989) 1963.

[18] S. Ishimoto, PhD thesis, The Graduate University for Advanced Studies, 1993, unpublished,

[19] T. O. Niinikoski *Nucl. Inst. Meth.* **97**, (1971) 95.

[20] R. Bernard, P. Chaumette, P. Chesny, J. Derégel, R. Duthil, J. Fabre, C. Lesmond, and G. Seité *Nucl. Inst. Meth.* **A249**, (1986) 176.

[21] D. Adams, et al., *Phys. Lett.* **B 329**, (1994) 399,

J. Kyynäräinen, *Nucl. Inst. Meth.* **A 356**, (1995) 47.

[22] D. L. Adams, et al., *Phys. Lett.* **B 336**, (1994) 269.

S. Makino, Memories of the Faculty of Science, Kyoto University Series of Physics, Astrophysics, Geophysics and Chemistry, Vol. XXXIX, No.2, (March 1995).

G. Durand, et al., Proceedings of the 9th International Symposium on High Energy Spin Physics, Bonn, 1990, Vol. 2, Workshop on Polarized Solid Targets, (Springer, Berlin, Heidelberg, 1991), p.237.

[23] V. I. Lushchikov, Y. V. Taran, and F. L. Shapiro, *Sov. J. Nucl. Phys.* **10**, (1970) 669.

[24] S. Hiramatsu, et al., *J. Phys. Soc. Jpn* **45**, (1978) 949.

[25] S. Ishimoto, et al., *Jpn. J. Appl. Phys.* **25**, (1986) L246.

[26] P. P. J. Delheij, et al., *Nucl. Inst. Meth.* **A 356**, (1995) 120,

[27] S. I. Penttilä, et al., Proceedings of the 11th International Symposium on High Energy Spin Physics, Bloomington, 1994, (AIP Press, Woodbury, New York, 1995) p.532.

[28] For example, see Proceedings of an International Symposium on *"The Triplet State"*, held at the American University of Beirut, Lebanon, 1967, edited by A. B. Zahlan, et al., (Chambridge at the University Press 1967).

[29] For example, see K. H. Hausser, and H. C. Wolf, *Advances in MAGNETIC RESONANCE*, **Vol. 8**, 1976, (Academic Press Inc. N.Y.), p.85.

[30] H. W. van Kesteren, W. Th. Wenckebach, J. Schmidt, and N. J. Poulis, *Chem. Phys. Lett.* **89**, (1982) 67.

[31] H. W. van Kesteren, W. Th. Wenckebach, and J. Schmidt, *Phys. Rev. Lett.* **55**, (1985) 1642.

[32] A. Henstra, P. Dirksen, and W. Th. Wenckebach, *Phys. Lett.* **A 134**, (1988) 134.

[33] A. Henstra, T.-S. Lin, J. Schmidt, and W. Th. Wenckebach, *Chem. Phys. Lett.* **165**, (1990) 6.

[34] D. J. van den Heuvel, Master thesis, Leiden, 1991, unpublished.

[35] M. S. de Groot, I. A. M. Hesselmann, J. Schmidt, and J. H. van der Waals, *Mol. Phys.* **15**, (1968) 17.

[36] W. S. Veeman and J. H. van der Waals, *Mol. Phys.* **18**, (1970) 63.

[37] D. J. Sloop, T. -L. Yu, T.-S. Lin, and S. I. Weissman *J. Chem. Phys.* **75**, (1981) 3746.

[38] A. J. Van Strien and J. Schmidt *Chem. Phys. Lett.* **70**, (1980) 513.

[39] Wim H. Hesselink and Douwe A. Wiersma, *Phys. Rev. Lett.* **43**, (1979) 1991.

[40] A. Henstra, PhD thesis, Leiden, 1990, unpublished.

[41] S. C. Abrahams, J. Monteath, and J. G. White, *Acta Cryst.* **2**, (1949) 238.

D. W. J. Cruickshank, *Acta Cryst.* **10**, (1957) 504.

[42] H. M. Rietveld, E. N. Maslen, and C. J. B. Clews, *Acta Cryst.* **B26**, (1970) 693.

[43] J. L. Baudour, Y. Delugeard, and H. Cailleau, *Acta Cryst.* **B32**, (1976) 693.

[44] T. Gullion and M. S. Conradi, *Phys. Rev. B* **31**, (1985) 4388.

[45] B. Toudic, J. Gallier, P. Rivet, and H. Calleau, *Solid State Commun.* **47**, (1983) 291.

[46] K. Kouda, N. Nakamura, and H. Chihara, *J. Phys. Soc. Jpn* **51**, (1982) 3936.

[47] H. Labhart and W. Heinzelmann, *Organic Molecular Photophysics* **Vol. 1**, (edited by J. B. Birks, John Wiley & Sons, 1973), 297.

[48] G. Porter and M. W. Windsor, *Proc. Roy. Soc.*, **A245**, (1958) 238.

[49] J. U. von Schuetz and H. C. Wolf, *Z. Naturforsch.* **27**, (1972) 42.

[50] J. Haupt, and W. Müller-Warmuth, *Z. Naturforsch.* **22a**, (1967) 643.

[51] O. Lauer, D. Stehlik and K. H. Hausser, *J. Mag. Res.* **6**, (1972) 524.

[52] M. Iinuma, I. Shaké, R. Takizawa, M. Daigo, H. M. Shimizu, Y. Takahashi, A. Masaike, T. Yabuzaki, *Phys. Lett. A* **208**, (1995) 251.

[53] M. Borghini, O. Chamberlain, R. Z. Fuzesy, W. Gorn, C. C. Morehouse, T. Powell, P. Robrish, S. Rock, S. Shannon, G. Shapiro, and H. Weisberg *Nucl. Inst. Meth.* **84**, (1970) 168.

[54] A. Thomas, Ch. Bradtke, H. Dutz, R. Gehring, S. Goertz, H. Hainer, W. Meyer, M. Plückthun, G. Reicherz, K. Runkel *Nucl. Inst. Meth.* **A 356**, (1995) 5.

[55] D. G. Crabb, D. B. Day, *Nucl. Inst. Meth.* **A 356**, (1995) 9.